Dynamical Climatology

Sensitivity of the Met O 20 11-layer model to increased land surface roughness length

by

C.C. Heasman

DCTN 49

February 1987

Meteorological Office (Met. O. 20)
London Road
Bracknell
Berkshire RG12 2SZ

DYNAMICAL CLIMATOLOGY TECHNICAL NOTE NO. 49

SENSITIVITY OF THE MET O 20 11-LAYER MODEL TO INCREASED LAND SURFACE ROUGHNESS LENGTH

by

C C Heasman

Met O 20 (Dynamical
Climatology Branch)
Meteorological Office
London Road
Bracknell
Berkshire, RG12 2SZ U.K.

February 1987

Note: This paper has not been published. Permission to quote from it should be obtained from the Assistant Director of the above Meteorological Office branch.

1. Introduction

Many experiments have been performed using the Met O 20 11-layer model (Saker 1975), with the aim of simulating the observed January circulation. These experiments fall into two classes, those which used fixed external forcing conditions appropriate to perpetual January, and those which used seasonally varying sea-surface temperatures, insolation, cloud amounts and ozone concentrations. The first class of experiment has been carried out on the IBM 360/195 computer and on the Cyber 205 computer (for example Heasman 1984, Rowntree and Mitchell 1982). The second class of experiment was performed on the Cray-1 computer at ECMWF (Cunnington 1983) and the Cyber 205.

All these integrations showed a tendency for the model to produce over-intense westerly flow in the Northern Hemisphere winter. This excessive westerly flow is associated with an inability of the model to simulate the observed partitioning of kinetic energy correctly (Rowntree 1983, Heasman 1984). Such flow is evident in charts of mean sea level pressure. These show that the model produces far too deep Aleutian and Icelandic lows, with associated troughs extending eastwards into the American and Eurasian continents. These charts also show that the model incorrectly simulates the position and strength of the Azores high, which is too far to the North-East and too strong. These characteristic features lead to low level flow which is too strong in the Northern Hemisphere mid-latitudes, particularly over Europe.

The problem of excessive westerly flow, particularly for the Northern Hemisphere winter, is not unique to the 11-layer model (Wallace et al 1983). Experiments by Wallace et al (1983) and by Wilson, H (1984) show that simulations produced by numerical models are sensitive to the specification of orographic height. Use of increased orography, or of an envelope orography, tended to reduce the intensity of the westerly flow, although it did not necessarily give a greatly improved simulation of the flow over the whole of the Northern Hemisphere.

The problem of excessive westerly flow seems to be greater for the Meteorological Office model than for the ECMWF model. This may be partly due to the use of vertical diffusion of momentum throughout all the model atmosphere in the ECMWF model, whereas momentum is only diffused vertically within the boundary layer in the Meteorological Office model.

Wilson and Slingo (1983) analysed the simulation of the January circulation in the European area. They suggested that the over deep Icelandic low produced by the 11-layer model may result from a poor simulation of the life-cycle of low pressure systems, with excessive troughing into northern Europe arising from insufficient 'filling' of depressions as they move inland. This may arise from a lack of friction over land surfaces.

The surface roughness length (z_o) can be considered as giving a measure of the influence of surface features on the low level flow. Friction at the surface of the earth arises both from variations in the local terrain height and from small-scale roughness elements, which may be determined by the land cover eg. forest, desert etc. There will generally be many sub-grid scale orographic features such as hills and valleys within the surface area covered by a typical GCM grid-box over land. These small

scale variations in the surface height introduce pressure differences and provide a 'form' drag on the atmosphere. Fiedler and Panofsky (1972) proposed that, in regions of variable terrain, one should use an effective roughness length z_o(eff) which is defined as that value which homogeneous terrain would require to give the same surface stress. They suggested values of 1.42 m for 'high' mountains, 0.99m for 'low' mountains and of 0.42m for 'plains'.

The 11-layer model currently uses roughness lengths of 0.0001 m over sea points, and 0.1m over all other points. As an initial step towards introducing a land surface roughness length which is dependent on sub-grid scale features, an integration was performed in which zo was increased to 1m for all land and land ice points. The control integration (WAZG) used roughness lengths of 0.0001 m over sea points and 0.1 m over all other points. The perturbation experiment (WAZF) used roughness lengths of 0.0001 m over sea points, 0.1 m over sea-ice points and 1 m over land and land-ice points. The physical parametrizations and other details of the integrations are summarised in Table 1.

The two integrations were carried out on the Cyber 205 computer. These runs used the 12Z fields for 27 December 1972 for initial conditions. The fields for days twenty-one to fifty, and for days fifty-one to eighty for each experiment were meaned to form the two thirty day means studied here. These thirty day means were then taken to provide two pairs of January simulations.

The method of calculating surface fluxes used by the model is described in the next section. Both integrations used the Clarke boundary scheme to calculate the turbulent fluxes. This scheme is discussed in

Heasman (1983). The global effect of changing the land surface roughness is described in Section 3, while Section 4 discusses the effect of this perturbation on the simulated European climate.

2. Calculation of surface fluxes

The fluxes of momentum, heat and moisture at the surface are calculated using Monin-Obukhov similarity theory. The vertical turbulent flux F_χ at the surface is given by

$$F_\chi = -C_\chi V(z) [\chi(z) - \chi_s] \qquad (1)$$

where C_χ is the bulk transfer coefficient, V(z) is the wind speed at height z - taken to be the lowest layer of the model - and $\Delta\chi(z)$ is the difference between the value of quantity χ at the lowest model level ($\chi(z)$) and the surface value χ_s.

The specification of surface layer bulk transfer coefficients from Monin-Obukhov similarity functions is given in Carson and Richards (1978) and Carson (1982a), so only a brief description of its implementation in the 11-layer model will be given below.

The bulk transfer coefficient C_χ can be expressed in terms of the functions Φ_χ, which are calculated from the Monin-Obukhov similarity functions (ϕ).

$$C_\chi = k^2 \Phi_m^{-1}(\zeta,\zeta_s) \Phi_\chi^{-1}(\zeta,\zeta_s) \qquad (2)$$

where $\zeta = z/L$, z is the vertical coordinate and L is the Monin-Obukhov length (see Carson 1982a p88) and k is von Karman's constant. The bulk transfer coefficients used by the 11-layer model are based on the relationships given below, where ϕ is assumed to be the same for heat and moisture.

In stable conditions ($z/L > 0$ and $RIB > 0$) the following relations, of Webb (1970), are used for the Monin-Obukhov function

$$\phi_m = \phi_H = \phi_w = 1 + 5z/L \qquad 0 < \frac{z}{L} \leq 1$$
$$= 6 \qquad 1 < z/_L < 6 \qquad (3)$$

A limiting value is set on the value of the drag coefficients used in stable conditions enabling extension of the above formulae into very stable conditions, as discussed in Carson (1982a).

In unstable and neutral conditions ($^z/_L \leq 0$ and $RIB \leqq 0$) the model uses the relationships proposed by Dyer and Hicks (1970),

$$\phi_m = (1 - 16z/L)^{-1/4} \qquad 0 \geq \frac{z}{L} \geq -1$$
$$\phi_H = \phi_w = (1 - 16z/L)^{-1/2} \qquad (4)$$

The quantity ζ is not a function of known model variables $V(z)$ and $\Delta\chi(z)$, so, as discussed by Carson and Richards (1978, p.71), the bulk Richardson number for the layer from the surface to height z is used instead as a 'measure' of stability, where

$$RIB = \frac{gz\,[\Delta\theta(z) + .61\,T(z)\,\Delta q(z)]}{T\quad V^2(z)} \qquad (5)$$

where the temperature (T) and wind (V) are evaluated for the lowest model level, and the differences in potential temperature ($\Delta\theta$) and in moisture (Δq) are calculated between the lowest model level and the surface. In dry conditions (soil moisture content (SMC) < 5cm) the surface cannot be considered to be saturated, and the moisture difference is limited according to

$$\Delta q = 0.2\ SMC\ (q(z) - qsat(T_s)) \qquad (6)$$

where qsat (T_s) is the saturation specific humidity at the surface for the surface temperature T_s.

In freely convecting conditions

$$C_H \propto |RIB|^{1/2} \qquad \text{(Carson 1982a)} \qquad (7)$$

In the 11-layer model, the functional dependence of C_χ on RIB is empirically and smoothly extrapolated from the values given by the Dyer and Hicks formulae onto the free convective form for large negative RIB. The surface stresses are normally quite small in highly unstable conditions, so C_D is assumed constant beyond some empirically determined value of RIB. This method leads to C_H (and C_W) > C_D in unstable conditions.

This is illustrated in Figure 1, which shows bulk transfer coefficients for momentum (C_D) and for heat and moisture (C_H) as a function of bulk Richardson number for the values of land surface roughness used in these experiments. This figure illustrates how the 'influence' of the surface is increased for WAZF, through the increase in C_D and C_H with roughness length.

The standard version of the 11-level model on the Cyber 205 uses a look-up table containing bulk transfer coefficients as a function of bulk Richardson number. This table assumes that the roughness length of sea points is 0.0001 m and that of all other points is 0.1 m. To perform integrations with different roughness lengths it was thus necessary to change the model boundary layer scheme so that the bulk transfer coefficients could be calculated as a function of both bulk Richardson number and surface roughness. This code then had to be 'vectorised' so that it could be run efficiently on the Cyber 205.

3. Results

3a. Mean sea level pressure

The main features of the simulated pressure field are illustrated in Figure 2, which shows the zonal mean sea level pressure (PMSL) for the two thirty day means of the control integration (WAZG) and the perturbation experiment (WAZF). This figure also shows the climatological zonal mean pressure of Schutz and Gates (1971), which has minimum pressures of 1014 and 989 mb in the Northern and Southern Hemispheres respectively. Figure 2 shows that the 11-layer model does not correctly simulate these low pressure belts in integrations with fixed external forcing conditions, although the Southern Hemisphere low pressure belt is well simulated in experiments with seasonally varying forcing (Cunnington 1983).

The effect of increasing the land surface roughness on the Northern Hemisphere mid-latitude zonal mean PMSL varies between the two thirty day means. For the first thirty day mean, the low pressure belt is less intense and in a more southerly position for WAZF. The reverse is seen for the second thirty day mean.

In the Southern Hemisphere, the depth of the low pressure belt is little changed between the control and the perturbation experiments. The simulation of the position of the low pressure belt is poorer for WAZF, which gets the minimum pressure in a more northerly position. The lack of sensitivity in the Southern Hemisphere to changing z_o over land, reflects the lack of land in the low pressure belt region of this hemisphere. WAZF consistently has lower pressure in the tropics and higher pressure in the Northern Hemisphere sub-tropical high pressure belt.

More detail about the impact on the global pressure pattern of changing land surface roughness is given in Figure 3. Figures 3a-3f show global fields of PMSL, and of their differences, for the two thirty day means. Figure 3g shows the January climatological PMSL field, produced by Schutz and Gates (1971). Shading on the fields of PMSL indicates regions of high (>1020 mb) and of low (<1000 mb) pressure. Shading on the difference maps indicates regions where WAZF has a lower pressure than WAZG.

Figures 3c and 3f show that there are some consistent differences between the PMSL fields produced by the two experiments. Increasing the land surface roughness has raised the pressure over eastern Canada, the USA and East Pacific and over the Northern Hemisphere subtropical Atlantic, and has reduced the pressure over most of the tropics. The PMSL fields in the almost land-free Southern Hemisphere show little sensitivity to the land surface roughness, although the low pressure belt is in a slightly more northerly position for WAZF.

Figures 3a-3f show that WAZF produces a better simulation of the Aleutian low for both thirty day means, producing pressures which are up to 8 mb higher. WAZF2150 has a more realistic simulation of the pressure distribution in the North Atlantic and North-Western Russia, despite having a more intense Icelandic low, with reduced troughing into the continent to the East. WAZF produces a poorer PMSL simulation for the second thirty day mean, getting a very deep Icelandic low, with extensive troughing eastward aross most of northern Russia. The sensitivity of the PMSL field over Europe to changing z_o will be considered in section 4.

The Siberian high extends further north for WAZF2150 than for WAZG2150. The extent of this high is reduced and is similar, for both WAZG5180 and WAZF5180. The 'Azores' high is stronger for WAZF5180 than for WAZG5180. WAZF consistently produced a stronger subtropical high across the United States and into the Eastern Pacific (by at least 5 mb).

Figures 2 and 3 show that 30 day mean PMSL fields are sensitive to the land surface roughness. However, these figures give no information about the day to day simulation of PMSL i.e. about the typical behaviour of depressions. It is thus useful to consider the behaviour of intense cyclonic features. It is assumed that this can be investigated by studying the temporal evolution of the deepest lows in three regions - in the North Atlantic and Eurasia to the east, in the North Pacific and America to the east, and in the Southern Hemisphere. Time series of the deepest low each day in each of these areas are shown in figures 4a, 4b and 4c. Figure 4a illustrates the tendency of the Icelandic low to become more intense during the later stages of the integrations, with minimum pressure never exceeding 980 mb during the second half of the integrations. In contrast, the depth of the Aleutian low (Figure 4b) decreases during the first 30 days of the integrations, but appears to reach an equilibrium (close to the original depth) during the last 20 to 30 model days. This behaviour is more evident for WAZF. Figure 4c shows that the minimum pressure in the Southern Hemisphere depression belt is relatively insensitive to land surface roughness, and is greater during the later stages of both integrations. This 'relaxation' has occurred after the first twenty days for both integrations.

This result, and the ones discussed above for the Northern Hemisphere, are shown more clearly in Figures 5a to 5f. The pressure of the deepest low in each region for each of days 21 to 50 and days 51 to 80 has been used to construct the histograms shown in Figures 5a to 5f. Figures 5a and 5d illustrate the increase in the depth of Atlantic lows with time, for the frequency distributions shift to lower pressures as the integrations proceed. This deepening with time is most pronounced for WAZF, with Figure 5d clearly showing that WAZF produced stronger lows during the last thirty model days of the integration. Figures 5b and 5e suggest, as noted earlier, that the North Pacific depressions become less intense during the last thirty days of the integrations. These figures also show that WAZF has less intense depressions in the Northern Pacific. By contrast, the Figures 5c and 5f indicate that the land-free Southern Hemisphere low pressure belt is relatively insensitive to the values of land surface roughness.

3b. Surface stress

Figures 6a - 6f show global fields of mean (accumulated) surface stress (τ) for the two experiments, and for their differences. These figures are in dynes/cm^2 (with a contour interval of 0.5 dynes/cm^2) (1 dynes/cm^2 = 0.1 Nm^{-2}); shading on the maps of τ indicate regions of low (<.5 dynes/cm^2) surface stress and shading on Figures 6c and 6f indicates regions where the difference in stress is less than 0.5 dynes/cm^2. The arrows indicate the direction of the stress/stress - difference. Figure 6g shows climatological values of τ over sea points (Han and Lee 1981). This climatology shows, in agreement with the surface flow, that the surface stress has its maxima in the depression belts. These maxima exceed 2

dynes/cm^2 in both hemispheres. The climatology has its maximum easterly component in the tropics, with magnitudes exceeding 1.5 dynes/cm^2 in the tropical Atlantic, and much of the western tropical Pacific.

Figures 6 show that the model simulates the main features of the observed surface stress, producing maximum westerly stress in the depression belts and easterly stress in the tropics and polar latitudes. The characteristics of the fields of τ generated by the model are in agreement with those of the model PMSL fields, discussed above. Thus, the model positions the 'North Atlantic' maximum too far to the east - over Europe rather than in mid-Atlantic. The stress over the North Atlantic is weaker than observed for the first thirty day means, and is comparable in magnitude with climatology ($\approx$ 2.5 dynes/cm^2) for the second thirty day means. The stress is simulated better in the North Pacific, where the model fields agree well with Han and Lee (1981). Both integrations have a region of low surface stress (<.5 dynes/cm^2) in tropical latitudes which extends almost completely around the globe. The climatological surface stress has low stress in the tropical Atlantic, Indian and Western Pacific, but does not show a pronounced minimum in the tropical East Pacific. The integrations all underestimate the magnitude of the Southern Hemisphere maxima. The climatological surface stress in the vicinity of Antarctica is based on few observations and thus has limited validity, so comparisons between model derived and climatological surface stress can only suggest that the integrations produce excessive easterly stress over the Antarctic sea ice shelf.

These features are summarised in Figures 7 and 8, which show the zonal mean surface zonal stress (in dynes/cm^2) for land and land-ice points (Figure 7) and for sea and sea-ice points (Figure 8). Figure 7 shows that

the surface zonal stress is most sensitive to increased land surface roughness in the depression belts and in the Northern Hemisphere subtropics. Figure 8 also shows the zonal mean surface zonal stress of Han and Lee (1981). This figure shows that, in agreement with the model PMSL fields, the model overestimates the magnitude of the Northern Hemisphere depression belt maximum, especially for days 51 to 80. Figure 8 also shows that the model underestimates the magnitude of the Southern Hemisphere depression belt maximum, and positions it about six degrees of latitude too far north.

Figures 6 to 8 show that the model simulates the main features of the observed surface stress. The characteristics of the model simulations are in agreement with those of the model PMSL fields, discussed above. Thus the model overestimates the magnitude of the Northern Hemisphere maxima and underestimates the magnitude of the Southern Hemisphere maxima.

Mitchell et al (1984) discussed the surface stress fields produced by a three year (seasonally varying) integration of the 11-layer model. They concluded that the model underestimated the surface stress, except in the Northern Hemisphere depression belt. The differences between their results and those described above cannot be attributed solely to differences in the surface pressure distribution, although the weaker easterly stress noted by Mitchell et al in the tropics is consistent with differences between the pressure fields produced by the two experiments (WAZF and WAZG consistently had a stronger northern subtropical high and stronger easterly winds), as both experiments produced similar, weak, surface stress in the Southern Hemisphere depression belt, (despite the 3 year integration having a much more realistic (deeper) low pressure belt). These results suggest, as discussed by Mitchell et al, that there may be an inherent problem with the

derivation of surface stress by the 11-layer model. This problem becomes more important with development of coupled ocean-atmosphere models, and suggestions for further work to improve the estimation of surface stress are made in section 6.

3c. Kinetic energy

Time series of global mean zonal kinetic energy (ZKE) and eddy kinetic energy (EKE) are given in Figure 9, which shows that the global kinetic energies for the two experiments differ by less than 3 J/kg for at least the first twenty days. This figure illustrates that ZKE for both experiments increases with time. EKE varies in a more complicated fashion with time. During the last 30 days of the experiment, the EKE for WAZF decreases with time. Figure 9 shows some evidence of energy conversions between EKE and ZKE, especially for WAZG. Note that the differences in ZKE between the two experiments tend to be out of phase with the differences in EKE.

These features are summarised in Table 2, which shows the partitioning of kinetic energy for the four thirty day means and for the January and February FGGE means (Rowntree and Mitchell 1982). These figures show that WAZF initially produces a better (reduced) simulation of the total kinetic energy. However the transient eddy kinetic energy is consistently greater for WAZG, by at least 3 J/kg. The zonal kinetic energy increases by 8 J/kg between days 21 to 50 and days 51 to 80 for WAZG and by 6 J/Kg for WAZF. Table 2 thus shows that increasing the land surface roughness consistently reduces the transient eddy kinetic energy and consistently increases the standing eddy kinetic energy.

3d. Zonal mean fields

Figures 10 and 11 show the zonal mean sensible heat fluxes (in W/m^2) from land and land-ice points (Figure 10) and from sea and sea-ice points (Figure 11). These figures show consistent differences in the sensible heat fluxes from land points between both pairs of thirty day means. The perturbation experiment has greater fluxes into the land between 30°N and 60°N, and slightly less at high latitudes in the Northern Hemisphere. WAZG has greater heat fluxes into the atmosphere in the southern tropics and between 40°S and 60°S. For some of these latitudes, the perturbation experiment has net sensible heat flux into the surface. The zonal mean sensible heat fluxes from sea points do not show consistent differences between experiments. Figure 10 shows that the sensible heat flux from the tropical maxima over land points increase with time (from ≈ 80 Wm^{-2} for the first 30 day mean to over 100 Wm^{-2} for the second 30 day mean). The sensible heat flux from Northern Hemisphere sea points has two maxima, at 35°N and at about 55°N. The subtropical maximum increases slightly with time. The 'depression' belt maximum increases and shifts northwards between the two successive thirty day means.

Figures 12 and 13 show the zonal mean evaporation (in mm/day) from land and land-ice points (Figure 12) or from sea and sea-ice points (Figure 13). These figures show that the evaporation from land points is greater for WAZF polewards of 40°N, for the equatorial maximum and in the Southern Hemisphere mid-latitudes. The perturbation experiment also produced slightly more evaporation from sea points in the Northern Hemisphere depression belt and in the Southern Hemisphere subtropics. The evaporation

from sea points has increased between the successive thirty day means for the Northern Hemisphere depression belt and in the Southern Hemisphere subtropics.

Comparison of figures 10 and 12 indicate that the changes in sensible heat flux between the two experiments are related to the evaporation, and the soil moisture. The 'total heat' flux (sensible heat flux plus latent heat flux) is approximately locally conserved over land. This is evident in the tropics, where the differences in zonal mean sensible heat flux between the pairs of thirty day means are in the opposite sense to the differences in evaporation. Also, in moist regions where the evaporation is greater for WAZF than for WAZG, the increased evaporation in the perturbation experiment reduces the, already small, temperature difference between the surface and the lowest model level. The small sensible heat flux in WAZG is thus reduced in WAZF. By contrast, in dry regions, where the evaporation is limited, the effect of increasing z_o will be more apparent in the sensible heat flux than in the evaporation. So, in regions which are dry for both experiments the sensible heat flux will be greater for the perturbation experiment. Such effects are discussed in more detail in Rowntree (1984).

Figures 14 and 15 show the zonal mean precipitation (in mm/day) over land and land-ice points (Figures 14) or sea and sea-ice points (Figure 15). Figure 14 shows that the precipitation over land points is consistently greater for the perturbation integration between 45°N and 65°N between 45°S and 55°S and in the Southern Hemisphere subtropics. The precipitation maxima over sea points in the tropics increase with time. The precipitation over sea points is greater for WAZF between 40°N and 60°N and in the Southern Hemisphere subtropics.

More detail about the geographical distribution of these differences is given in figures 16a and 16b, which show differences in precipitation between the two experiments. Shading on these figures indicates regions where WAZF had less precipitation than WAZG. These figures show that the precipitation differences are consistent with the pressure fields in the depression belts, with WAZF having more precipitation than WAZG in the Northern Hemisphere and similar amounts of precipitation in the Southern Hemisphere. The maps of precipitation differences are difficult to interpret in the Tropics, showing many small scale features which differ between the two thirty day means. This probably just reflects the 'noisiness' of the rainfall produced by the 11-layer model in the Tropics. There are some consistent features but longer experiments would be needed to establish statistical significance.

Figures 10 to 15 showed that increasing the surface roughness over land has produced changes in the zonal mean sensible heat flux, evaporation and precipitation which are consistent between the two thirty day means.

4. Sensitivity of the simulation in the European area

Figures 17a - 17f show PMSL fields, and their differences over the European area. Shading on these figures indicates regions of high (>1020 mb) or of low (<1000 mb) pressure. Shading on the difference maps indicates regions where WAZG has higher pressure than WAZF. The figures show that the flow across Europe remains similar between the two runs, being broadly westerly across the continent to at least 30°E.

Figure 17g shows a climatological PMSL field for January, which is derived from Meteorological Office Northern Hemisphere analyses for 1941 to 1970 (Benwell 1982). It can be seen from figures 17 that the simulated flow into Europe is stronger and has a weaker southerly component than is observed.

The simulation of PMSL over Europe is better for the first pair of thirty day means, which have a less developed Icelandic low. The pattern of the PMSL field is better simulated for WAZF2150 than for WAZG2150; WAZF2150 gets the 'Azores' high in a more southerly position, with lower pressure in the Mediterranean and a less extensive 'Azores' high and Icelandic low. However, the Icelandic low is less intense for WAZG2150. In contrast, WAZG5180 has a better simulation of the European PMSL field than WAZF5180, getting a less extensive and less intense 'Azores' high and Icelandic low. Both thirty day means produce a meridional pressure gradient over most of Europe. This gradient is stronger than observations for both thirty day means. The PMSL difference maps show, as mentioned above, that the differences between the thirty day mean fields reverse between successive thirty day means, so that no consistent signal is evident.

Figures 18a-18f show precipitation fields, and their differences, for the European area. Shading on the maps of precipitation indicates regions of more than 10mm/day. Shading on the difference maps shows regions where WAZG had more rainfall than WAZF. For comparison, Figure 18g shows a climatological precipitation field for January. The climatology shows a broad maximum over the North Atlantic, which extends along western Europe and through central Europe into the Mediterranean.

The rainfall patterns are similar for both pairs of thirty day means, which reproduce some, but not all, of the features noted above. Both integrations produce a relative maximum in precipitation over the Eastern Mediterranean but only the first pair of thirty day means obtain the observed maximum (>5 mm/day) over southern Italy and Sicily. The control integration is consistently wetter in this region. North of the Alps, the rainfall tends to decrease going inland to the east. This trend is weaker than observed, with all the model simulations producing more than 2 mm/day at 45°E 55°N, where the observations give between 1 and 2 mm/day. WAZF is consistently wetter than WAZG around 50°N and over most of eastern Europe. These differences exceed 2 mm/day in the vicinity of the UK and western France. Both integrations attempt to simulate the rain shadow area in the lee of the Norwegian mountains, such an effect is more pronounced for WAZF. The rainfall over southern Norway increases (improves) for the second thirty day means.

The fields of rainfall shown in Figure 18 are consistent with the model producing too intense lows and excessive westerly flow from the Atlantic into Europe. The differences between the patterns shown in Figures 18c and 18f are consistent with the European mean PMSL fields shown earlier. Thus for the first thirty day mean, where the Icelandic low was in a more southerly position for WAZF than for WAZG2150, WAZF2150 is wetter south of ≡ 53°N and WAZG2150 is wetter to the north. This pattern, in agreement with the PMSL fields, is switched for the second pair of thirty day means; thus WAZG5180 is wetter to the south of 50°N and WAZF5180 is wetter to the north.

5. Summary

As might be expected, the Northern Hemisphere showed greater sensitivity than the Southern Hemisphere to increasing the land surface roughness. The Atlantic/Eurasian and Pacific/North American sectors showed differing sensitivities to the applied perturbation. WAZF produced a better (shallower) simulation of the Aleutian low both for individual systems on a day to day basis, and for the two thirty day mean fields. WAZF also consistently produced higher pressure over much of North America and in the Eastern Pacific.

The Atlantic/Eurasian sector showed a less consistent response to increasing the land surface roughness. The first thirty day mean PMSL field suggested that increasing the land surface roughness had improved the simulation in the European area. Both experiments produced deeper Icelandic lows as the integrations proceeded. This deepening was more pronounced for the perturbation experiment, for which the minimum pressure in the Atlantic sector rarely exceeded 960 mb during the last twenty days of the integration. Thus WAZF5180 has a very deep Icelandic low, with extensive troughing into Eurasia to the East.

The simulated precipitation in the European area reflected the differences in the PMSL distributions. However, both experiments gave a reasonable simulation of the observed precipitation in Western and Southern Europe, and both experiments failed to get the observed decrease of rainfall towards Eastern Europe.

The zonal mean sensible heat flux, evaporation and precipitation all showed consistent differences between the two experiments. The evaporation from land points and the sensible heat fluxes into land points were consistently greater for the perturbation experiment between 40°N and 60°N.

The evaporation from the oceans in the Northern Hemisphere depression belt increased with time for both experiments, providing the moisture for the increase in precipitation between the two successive thirty day means in that region.

The simulation of the Southern Hemisphere showed little sensitivity to the applied perturbation. Both experiments got less intense depressions as the integrations proceeded. The position of the low pressure belt was better (more southerly) for the control integration.

6. Further experiments with changing surface roughness length

This note has shown that a January simulation by the 11-layer model is sensitive to land surface roughness, although the underlying problem of excessive westerly flow was not alleviated. Palmer and Shutts (1984) suggested that the orographic excitation of gravity waves and their consequent absorption above the boundary layer introduces a transport of momentum which damps the westerly flow. Using a 11-layer version of the Meteorological Office numerical forecast model, they added a simple parametrization of the orographic excitation of gravity waves and their absorption into the large scale flow above the boundary layer. They found that on using values of surface stress with magnitude exceeding 0.1 Nm^{-2}, a major improvement in the model climatology was obtained. This work is currently being extended to parametrize the vertical diffusion of momentum by gravity wave breaking and will be tested in the Met O 20 11-layer model in the near future. If these parametrizations produce a similar improvement in the simulations produced by the 11-layer model, then further experiments on the sensitivity of the model to surface roughness should produce clearer results.

Depressions usually tend to form and to spend most of their lifetime over the oceans, tending to decay over land. So, it is not unexpected that increasing the land surface roughness does not remove gross weaknesses in the simulation of the Northern Hemisphere winter circulation. With the development of a coupled ocean-atmosphere model, the need for a correct simulation of the surface stress over the oceans has increased.

At present, the 11-layer model uses a fixed value of roughness length over the sea. Charnock (1955) suggested, on dimensional considerations, that zo(sea) varied with surface wind speed according to the following formula

$$zo(sea) = \frac{M u_*^2}{g} = \frac{M C_D V^2}{g} \qquad (8)$$

where M is a constant, estimated by Charnock to be about 0.012, g is the acceleration due to gravity. The validity of such a formula was supported by Garratt (1977a), who concluded that observations of wind stress and wind profiles over the ocean are consistent with Equation (8).

Carson (1982b) conducted a small number of sensitivity experiments with a hemispheric version of the 11-layer model in which he used three different specifications of z_o (sea), including one based on the Charnock formula with M = 0.035. That study, which was limited to hemispheric, 7-day forecasting integrations and also the short-range forecasting of a specific storm-surge event in the North Sea, was inconclusive in the context of the need to have a wind speed dependent drag coefficient (or z_o) in a climate model. The Charnock formulation is currently being investigated further in a series of longer integrations with the full

11-layer atmospheric general circulation model. This will include the use of 0.0185 for M, a value established as appropriate for a wide range of wind speeds by Wu (1980, 1982).

The effective roughness length is also, but probably to a lesser extent, dependent on the vegetative land type within a model grid square. Garratt (1977b) gave the following expression for the impact of land surface cover on z_o

$$.02 < z_o/h < .2 \qquad (10)$$

where h is the height of the roughness elements (experimental data gave a geometric mean close to 0.06). Use of this relation gave the following values - 1 m for dense tropical rain forest, 0.1 m for mixed temperate forest, woodland or prairie and 10^{-4}m for extensive desert areas. A vegetation dataset has been produced for the 11-layer model (Wilson, M 1984). This dataset could be used, together with equation (10) to test the sensitivity of the model to 'vegetative roughness'.

Such experiments were proposed by Sud and Smith (1985), who investigated the sensitivity of the July circulation to the surface roughness of deserts. They reduced the surface roughness from .45m for land points to 2 x 10^{-4}m over deserts. They obtained a decrease in precipitation in the perturbation experiments, which they attributed to reduced moisture convergence into the region and to cooling of the boundary layer through increased longwave cooling.

The 11-layer model is being developed for use as a climate model, ie for long integrations to simulate possible climate perturbations of the effect of increasing CO_2. If such a perturbation produces a significant change to the earth's circulation patterns, the vegetation cover (and hence z_o(eff)) will change. The 11-layer model should thus have the potential to

use values of z_o(eff) which are dependent on the nature of the land surface, whether simply in terms of surface variables, or in terms of a diagnosed, or prognosed land use type.

Conclusion

The January circulation produced by the Met O 20 11-layer model is sensitive to the specification of land surface roughness. Increasing z_o improves the simulation near the Aleutians and the western United States, but does not remove the problem of excessive westerly flow.

Acknowledgements

This work was in part supported by the European Economic Community through the Programme of Research and Development in the field of climatology under contract CLI-031-UK(N), entitled 'European climate produced by an atmospheric general circulation model'. I should like to thank Dr P R Rowntree, Dr A Slingo and Mr H Wilson for their helpful discussions.

References

Benwell, P R 1982 Standard contour data sets. London, Met. Office, Met O 13 Data processing section Technical Note No. 7.

Carson, D J and Richards P J R 1978 Modelling surface turbulent fluxes in stable conditions. B.L. Met 14 67-81.

Carson, D J 1982a Current parametrizations of land-surface processes in atmospheric general circulation models. Land surface processes in general circulation models. Editor P S Eagleson, Cambridge University Press p.67-108. Also Met O 20 Technical Note II/152.

Carson, D J 1982b Comments on the Sensitivity of Numerical Simulations to Different Parameterizations of the Boundary-Layer Properties and Processes. Met O 20 Technical Note II/186.

Charnock, H 1955 Wind stress on a water surface. Q.J.R. Met. Soc. 81, 639-640.

Cunnington, W M 1983 An Annual-cycle integration of the 11-layer model. Met O 20 Technical Note II/212.

Dyer, A J and Hicks, B B 1970 Flux-gradient relationships in the constant flux layer. Q.J.R. Met. Soc. 96 715-721.

Fiedler, F and Panofsky, H A 1972 The geostrophic drag coefficient and the 'effective' roughness length. Q.J.R. Met. Soc. 98 213-220.

Garratt, J R 1977a Review of drag coefficients over oceans and continents. MWR 105 915-929.

Garratt, J R 1977b Aerodynamic roughness and mean monthly stress over Australia. Tech paper No 29 CSIRO Div. Atmos. Phys.

Han, Y -J and Lee, S -W 1981 A new analysis of monthly mean wind stress over the global ocean. Climatic Research Institute Report No. 26. Climatic Research Institute and Department of Atmospheric Sciences, Oregon State University.

Heasman, C C 1983 Boundary layer schemes used in the Met O 20 11-layer model. Met O 20 Technical Note II/215.

Heasman, C C 1984 The sensitivity of the 11-layer model to boundary layer parametrization schemes. Met O 20 Technical Note II/219.

Jaeger, L	1983	Monthly and areal patterns of mean global precipitation. Variations in Global Water Budget, Dordrecht.
Lyne, W H and Rowntree, P R	1976	Development of a convective parametrization scheme using GATE data. Met O 20 Technical Note II/70.
Mitchell J F B, Wilson C A, and Price C M	1984	On the specification of surface fluxes in coupled atmosphere ocean general circulation models. Met O 20 DCTN No 7.
Palmer, T N and Shutts, G S	1984	Preliminary results of the effect of a parametrization of gravity wave drag in the Meteorological Office 11-layer operational model. Met O 13 Branch Memorandum No 149.
Richards, P J R	1977	A comparison of an interactive radiation scheme and one based on climatology for use in the high-resolution model. Met O 20 Technical Note II/98.
Rowntree, P R	1983	Eddy kinetic energies in July integrations with the Meteorological Office general circulation model. Met O 20 Technical Note II/204.

Rowntree, P R 1984 Review of general circulation models as a basis for predicting the effect of vegetation change on climate. Met O 20 Technical Note II/225.

Rowntree, P R and Mitchell, J F B 1982 Preliminary analysis of 50-day integrations of the Met O 20 Cyber model. Met O 20 Technical Note II/194.

Saker, N J 1975 An 11-layer general circulation model. Met O 20 Technical Note II/30.

Schutz, C and Gates, W,L 1971 Global climatic data for surface, 800 mb, 400 mb: January. R-915-ARPA, Rand, Santa Monica, California.

Sud, Y C and Smith W E 1985 The influence of deserts on the July circulation. B.L. Met 33, 15-49.

Wallace, J M, Tibaldi, S and Simmons A J 1983 Reduction of systematic errors in the ECMWF model through the introduction of an envelope orography. Q.J.R. Met. Soc 109, 683-717.

Webb, E K 1970 Profile relationships: the log-linear range, and extension to strong stability. Q.J.R. Met. Soc., 96, 67-90.

Wilson, H 1984 The effects on the January circulation of the 11-layer model due to increasing orographic heights. Met O 20 Technical Note II/223.

Wilson, H and Slingo, A 1983 A study of the January climatology of the 11-layer model over the European area, Met O 20 Technical Note II/214.

Wilson, M F 1984 The construction and use of land surface information in a general circulation climate model. Phd thesis, University of Liverpool.

Wu, J 1980 Wind-stress coefficients over sea surface near neutral conditions. A revisit. J. Phys. Oceanogr., 10, 727-740.

Wu, J 1982 Wind-stress coefficients over sea surface from breeze to hurricane. J.G.R., 87 No C12, 9704-9706.

TABLE 1

Details of integrations

Initial conditions	12Z 27 December 1972
Model Grid	2.5 x 3.75 degrees
Time Step	10 minutes
Stability control	lateral diffusion of u,v,q,$aT + b\theta$
Physical parametrisation	
Boundary layer processes	Clarke (Heasman 1983)
Convective processes	Penetrative convection (Lyne and Rowntree 1976)
Radiative processes	Climatological radiation (Richards 1977)

TABLE 2

Partitioning of kinetic energy

	KS	KT	K	KZ	KE/K
WAZG2150	32.3	34.7	165.9	98.9	.40
WAZF2150	35.2	31.1	165.3	99.0	.40
WAZG5180	27.7	38.0	173.6	107.8	.38
WAZF5180	33.7	31.2	169.5	104.6	.38
FGGE JAN	20	54	150	76	.49
FGGE FEB	18	54	147	75	.49

KS = eddy kinetic energy of time meaned flow (standing eddy kinetic energy)

K = time averaged total kinetic energy

KE = time averaged eddy kinetic energy

KT = KE - KS = transient eddy kinetic energy

KZ = K - KE = K - KS - KT = zonal kinetic energy.

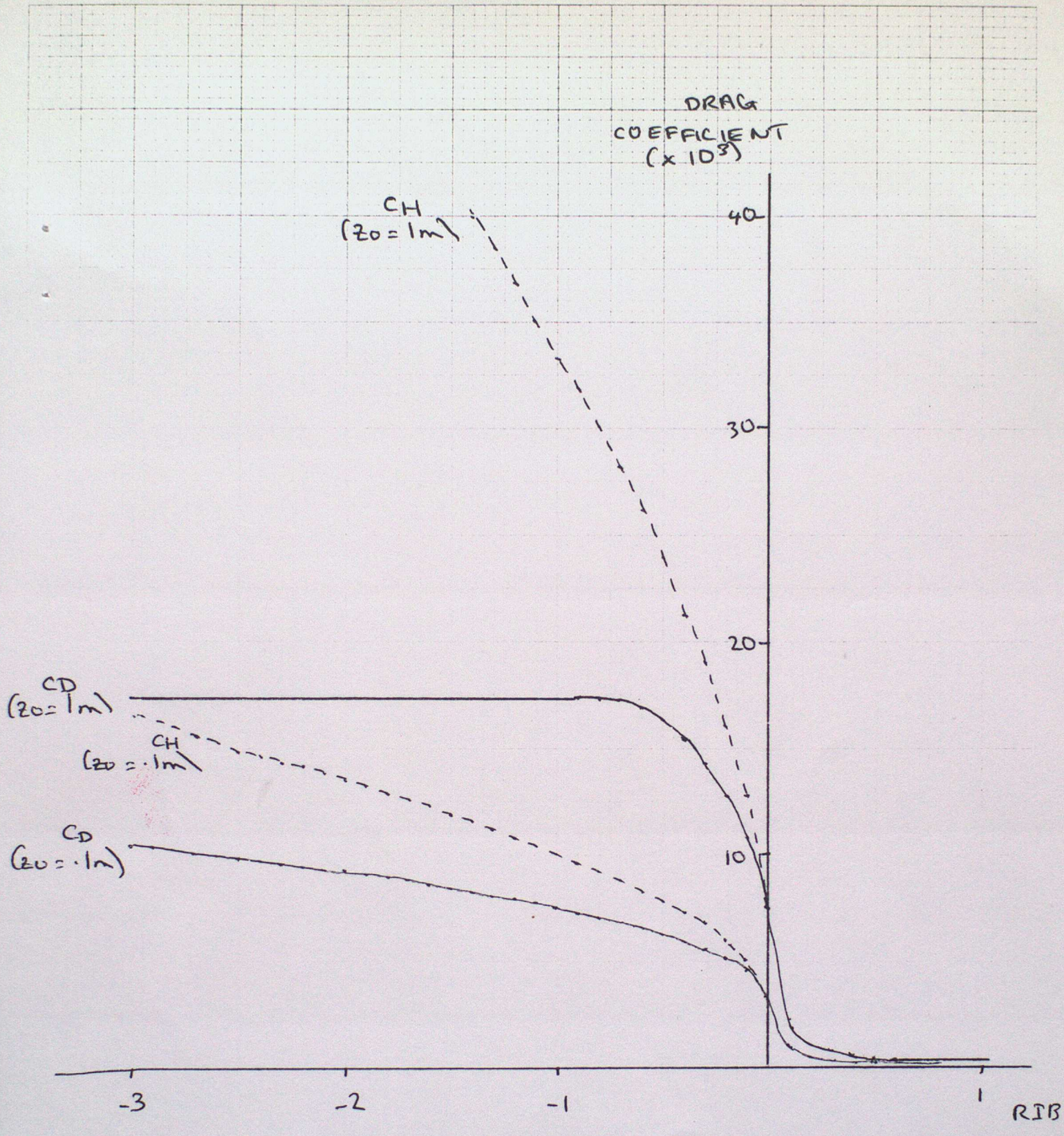

Figure 1: Bulk transfer coefficients as a function of bulk Richardson number.

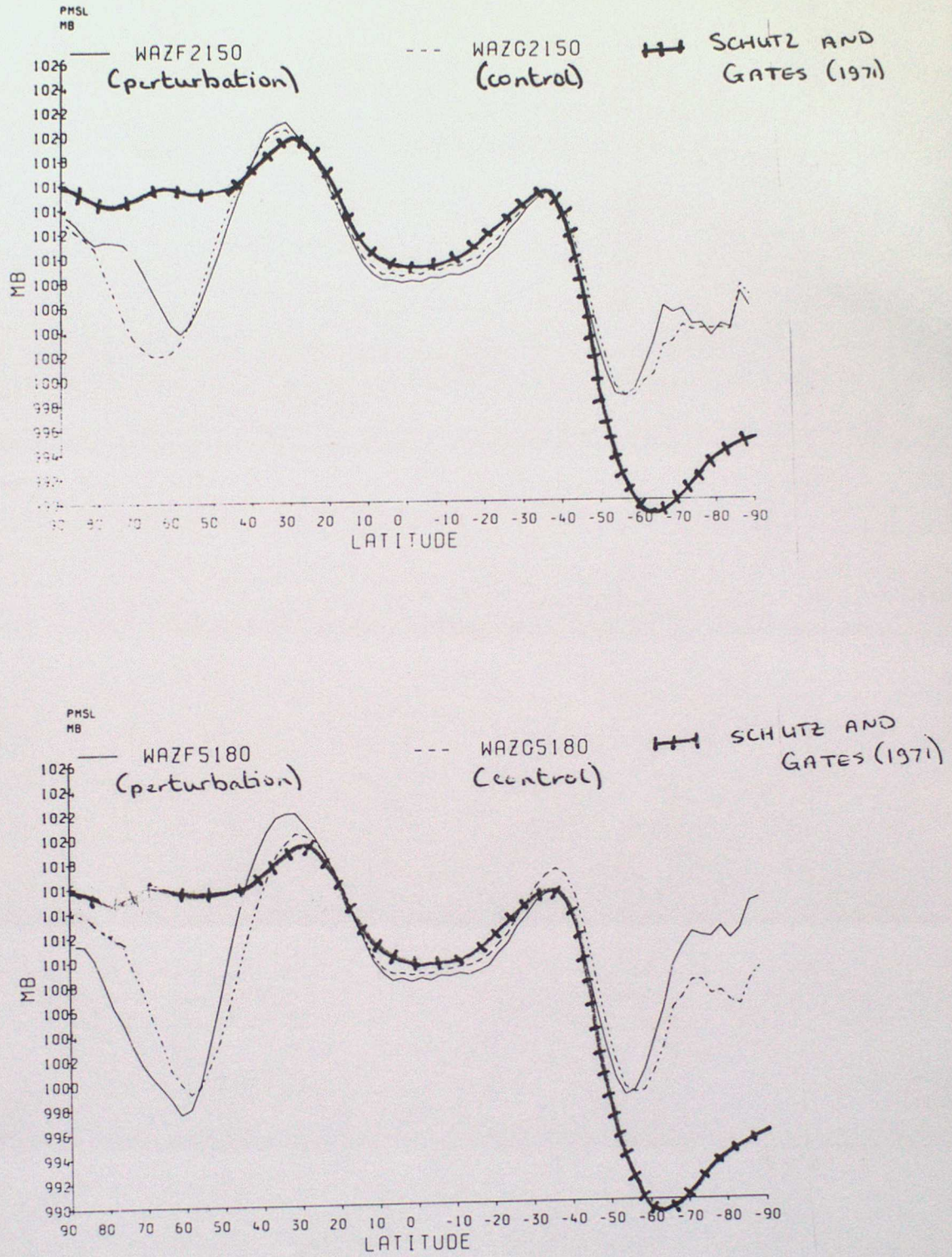

Figure 2: Zonal mean PMSL .

AVERAGE FROM OZ ON 2/12 DAY 21 TO OZ ON 1/1/1 DAY 50
LEVEL: SEA LEVEL EXPERIMENT NO.: 1231

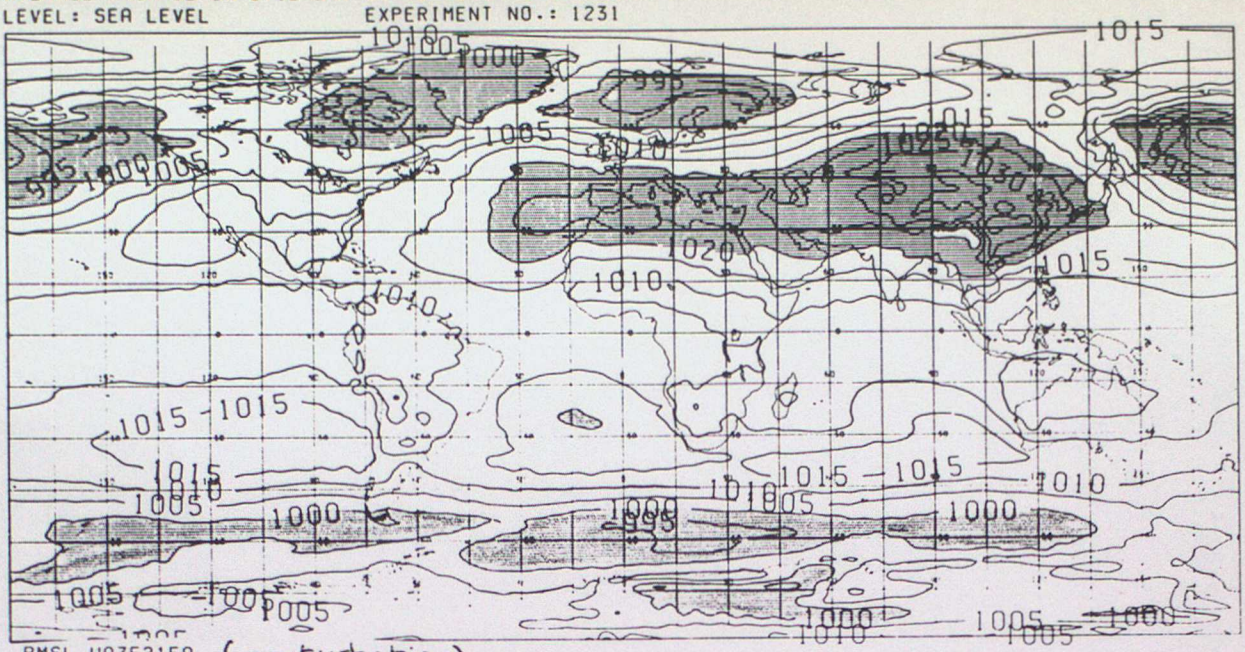

PMSL.WAZF2150 (perturbation)
AVERAGE FROM OZ ON DAY 21 TO OZ ON DAY 50
LEVEL: SEA LEVEL EXPERIMENT NO.: 1230

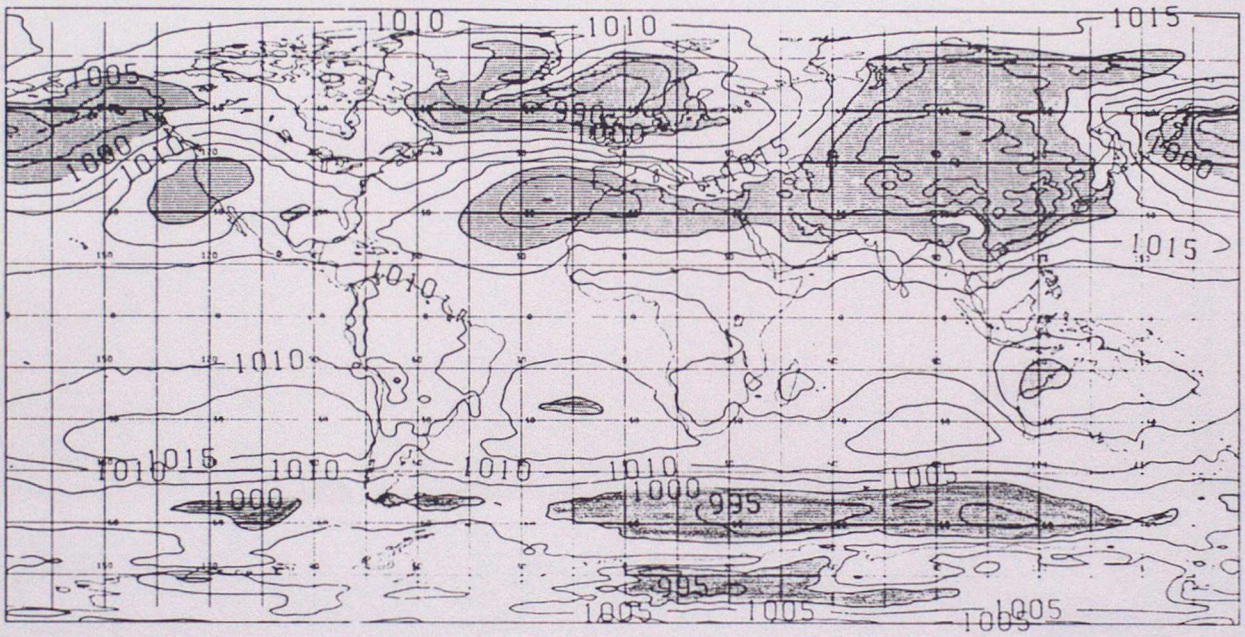

WAZF2150 - WAZG2150
MEAN SEA LEVEL PRESSURE
VALID AT OZ ON DAY 50
LEVEL: SEA LEVEL EXPERIMENT NO.: 1230

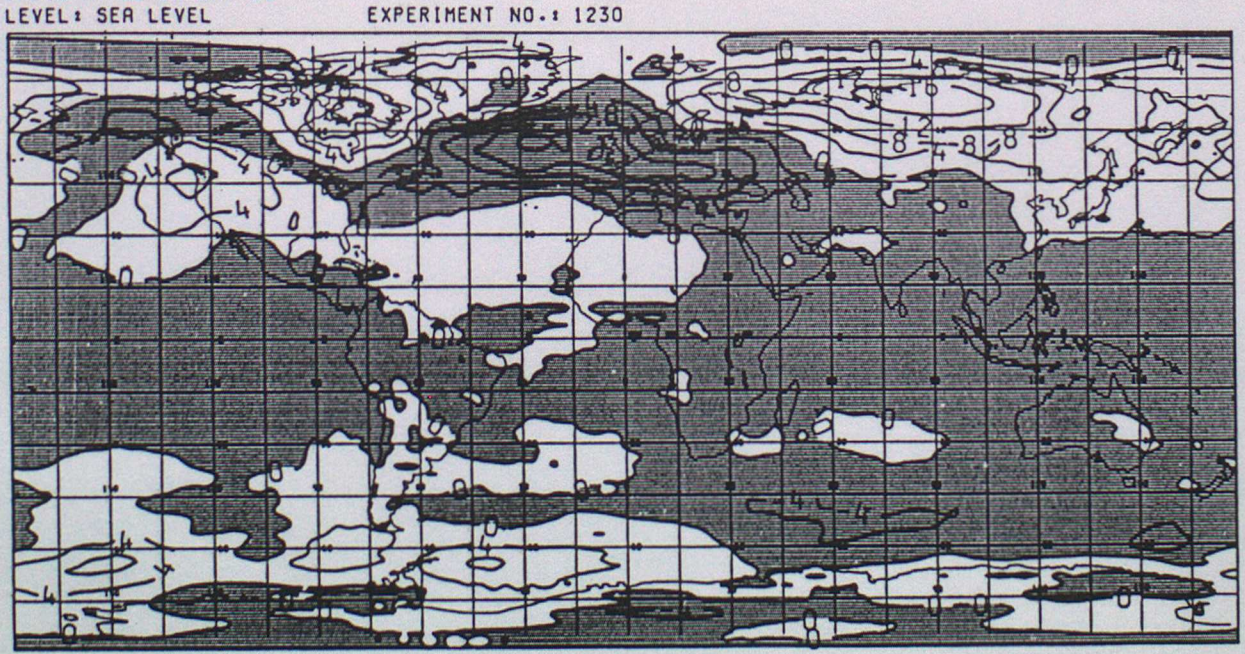

Figure 3: Global PMSL, a) WAZG2150, b) WAZF2150, c) WAZF2150 - WAZG2150.

AVERAGE FROM OZ ON 2/12 DAY 51 TO OZ ON 1/1/1 DAY 80
LEVEL: SEA LEVEL EXPERIMENT NO.: 1231

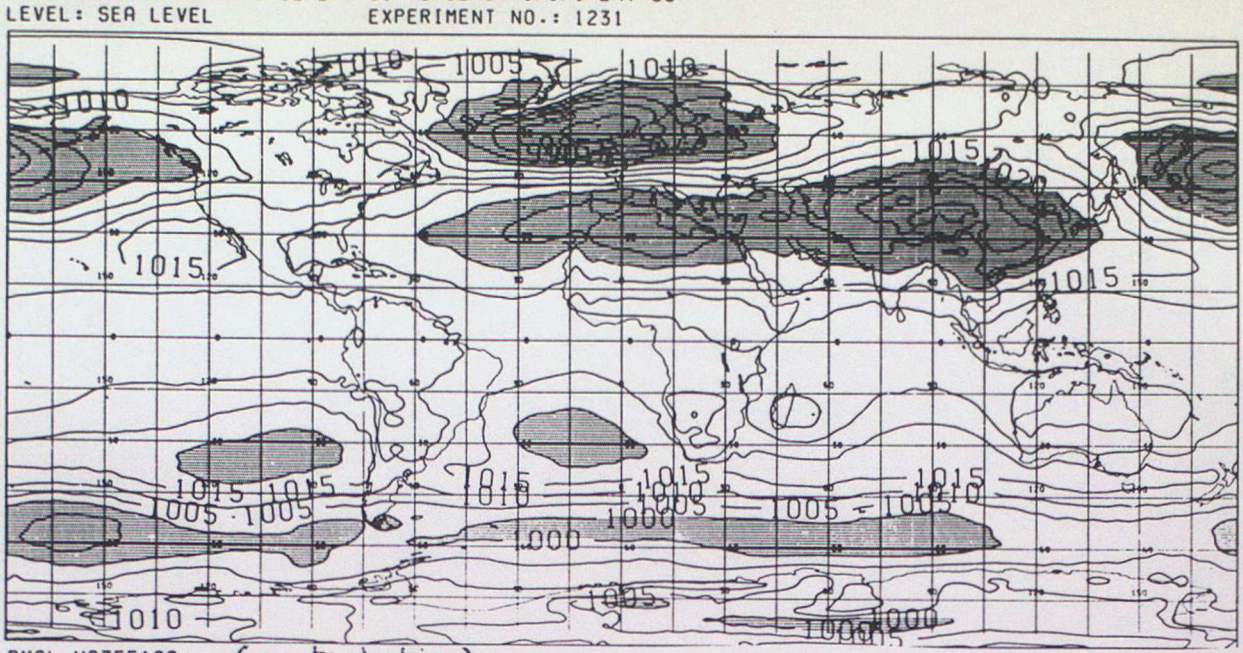

PMSL.WAZF5180 (perturbation)
AVERAGE FROM OZ ON DAY 51 TO OZ ON DAY 80
LEVEL: SEA LEVEL EXPERIMENT NO.: 1230

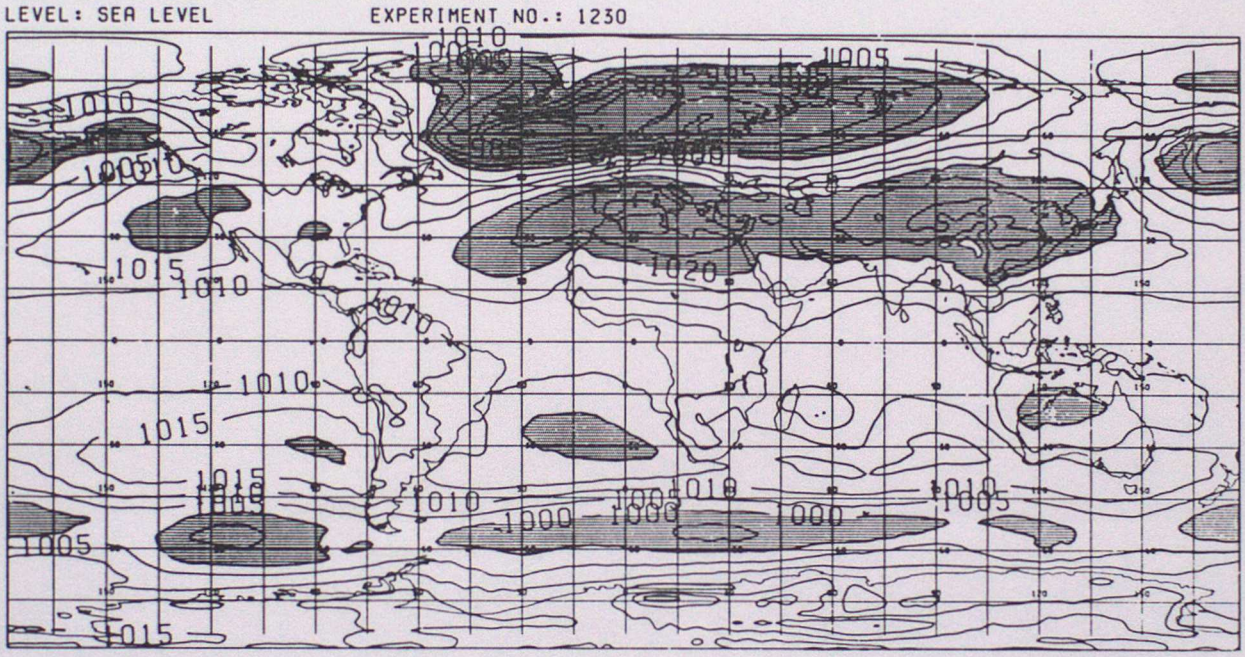

WAZF5180 - WAZG5180
MEAN SEA LEVEL PRESSURE
VALID AT OZ ON DAY 80
LEVEL: SEA LEVEL EXPERIMENT NO.: 1230

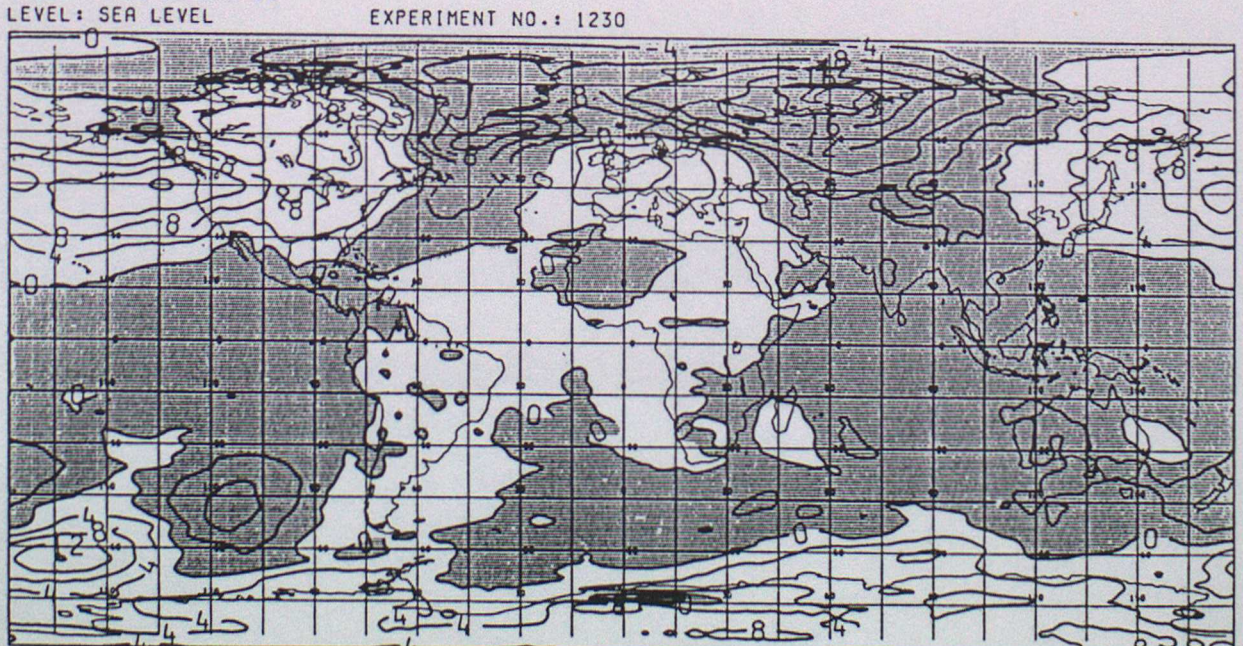

Figure 3: Global PMSL, d) WAZG5180, e) WAZF5180, f) WAZF5180 - WAZG5180.

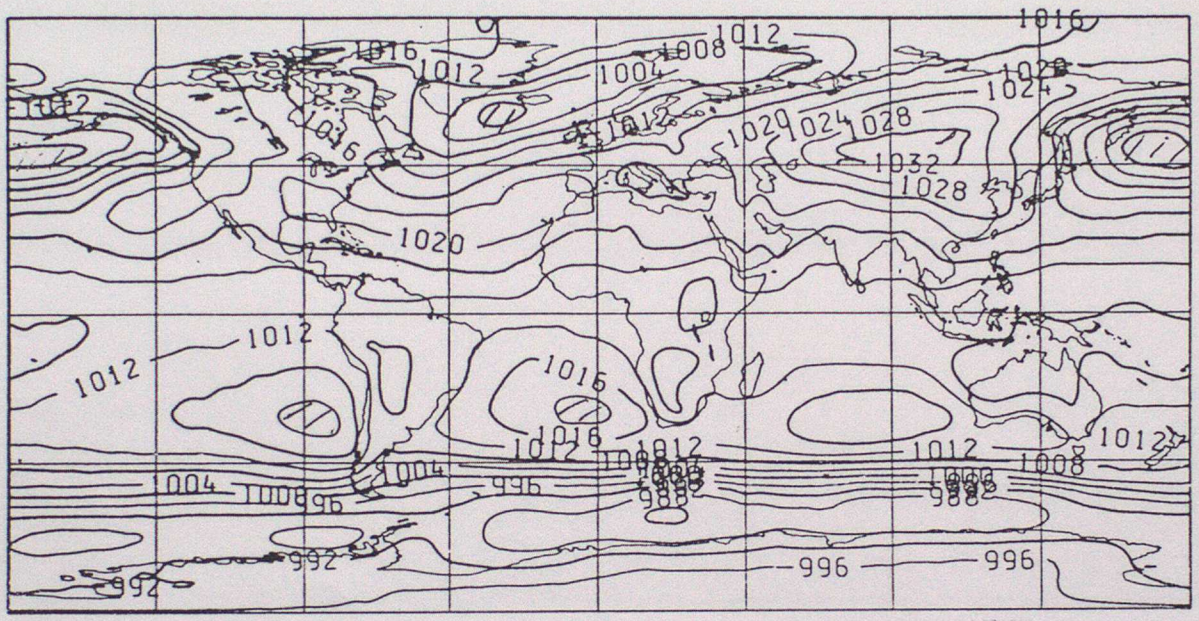

Figure 3: Global PMSL, g) Climatology (Schutz and Gates 1971).

Figure 4a: Depth of deepest low in Atlantic.

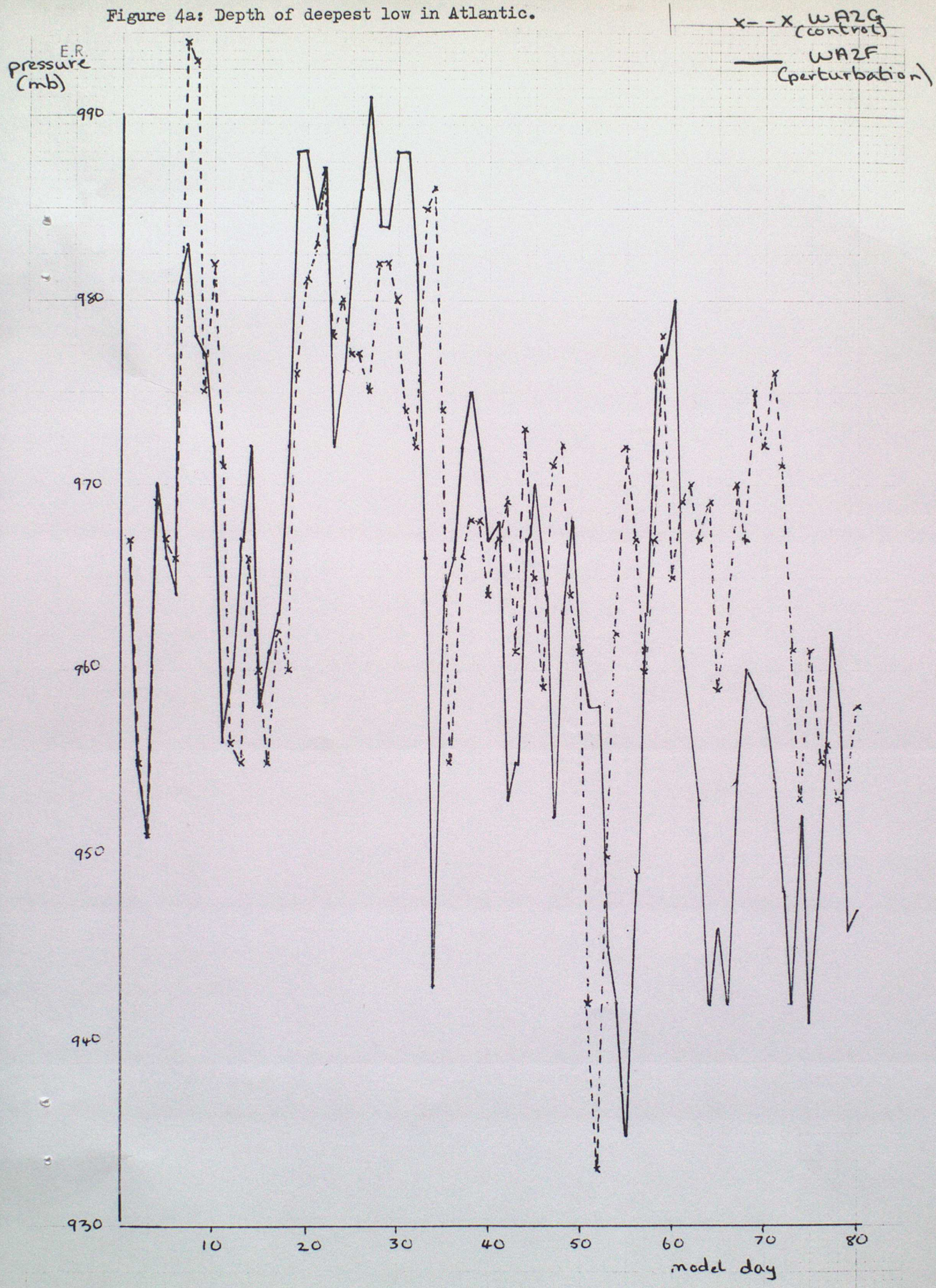

Figure 4b: Depth of deepest low in Pacific.

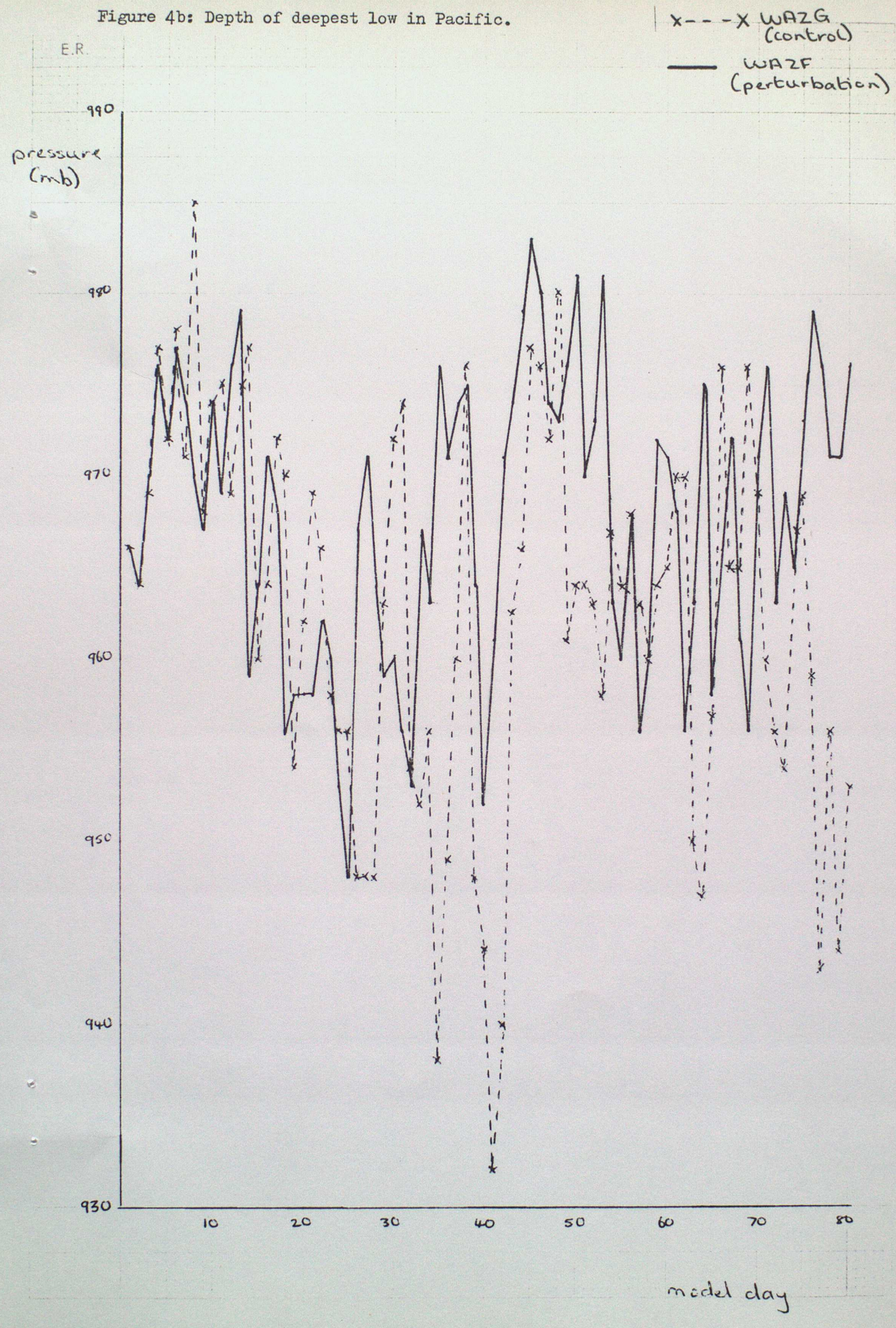

Figure 4c: Depth of deepest low in Southern Hemisphere.

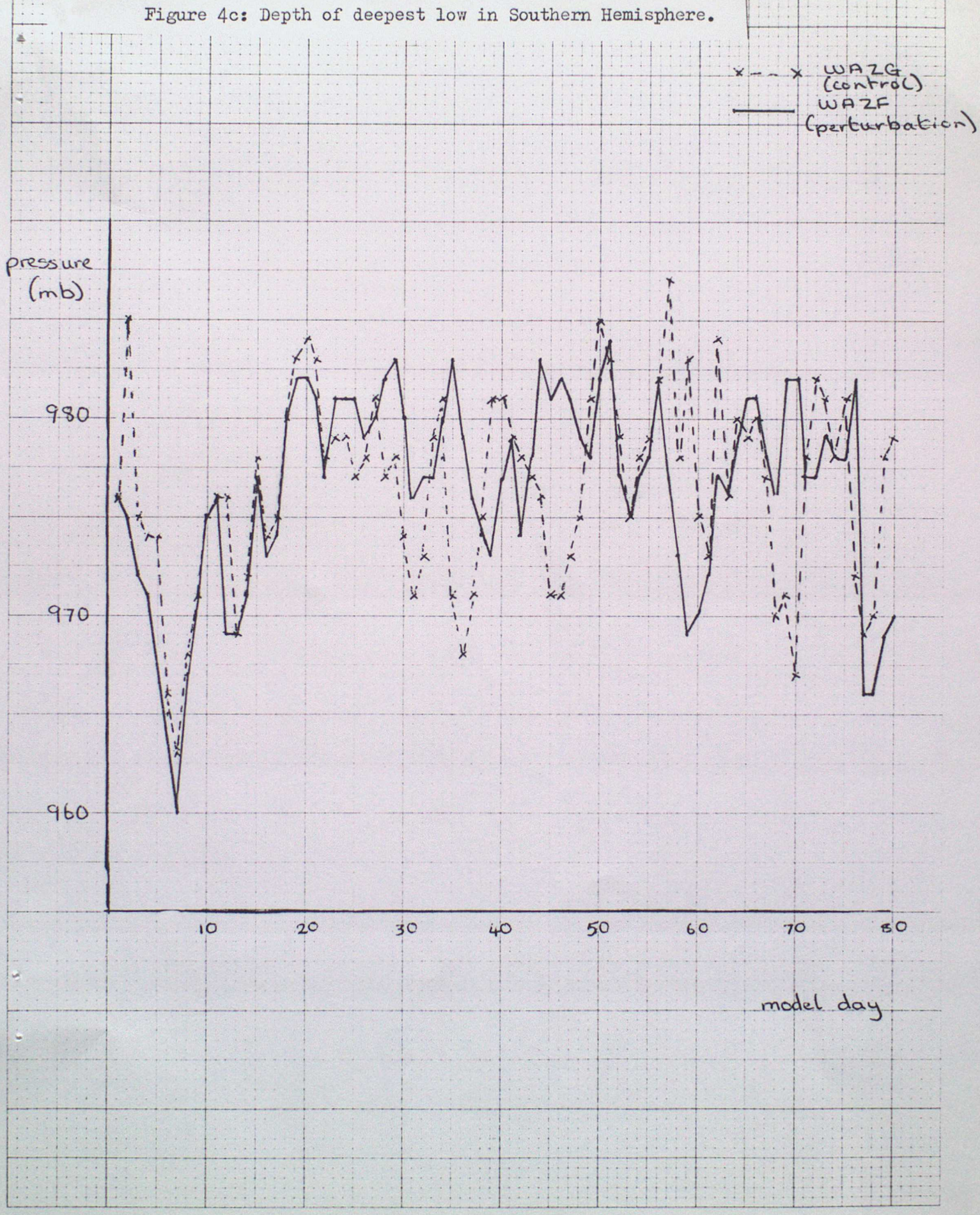

Figure 5: Histogram of occurrence of deepest low for days 21 to 50.

E.R.

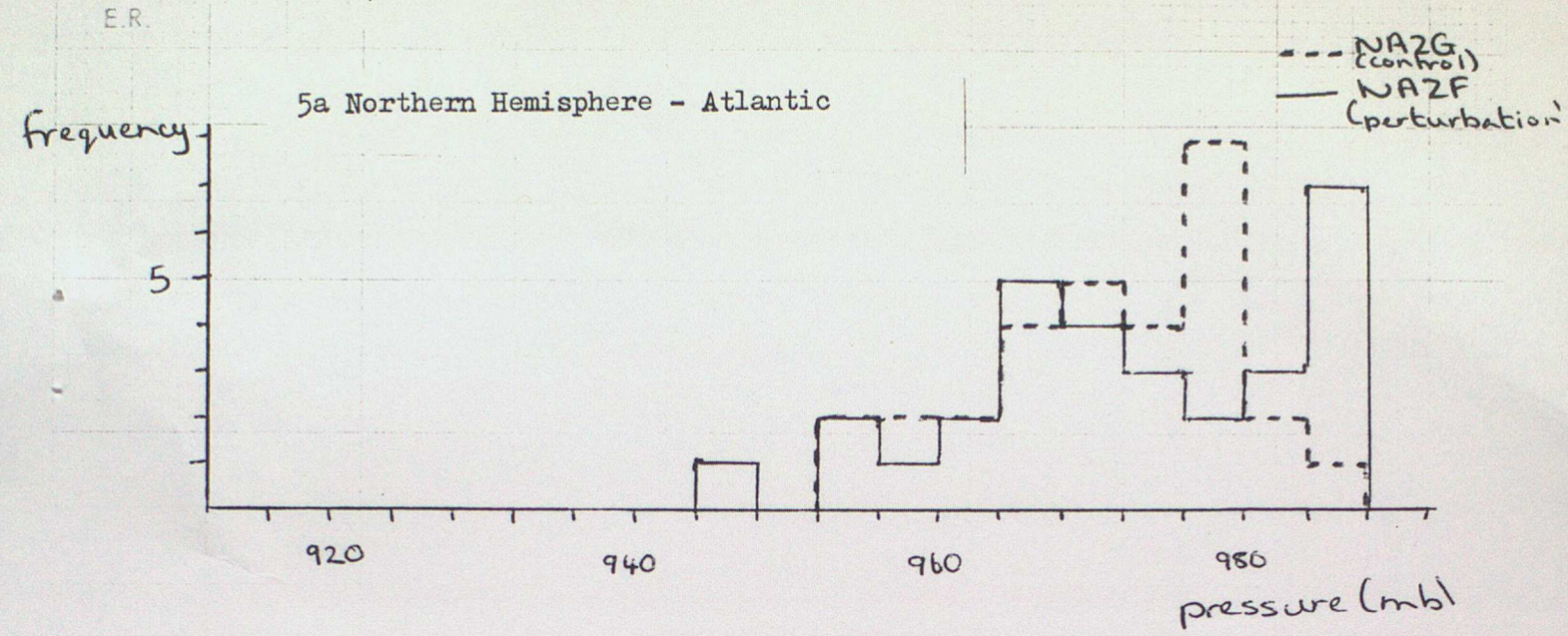

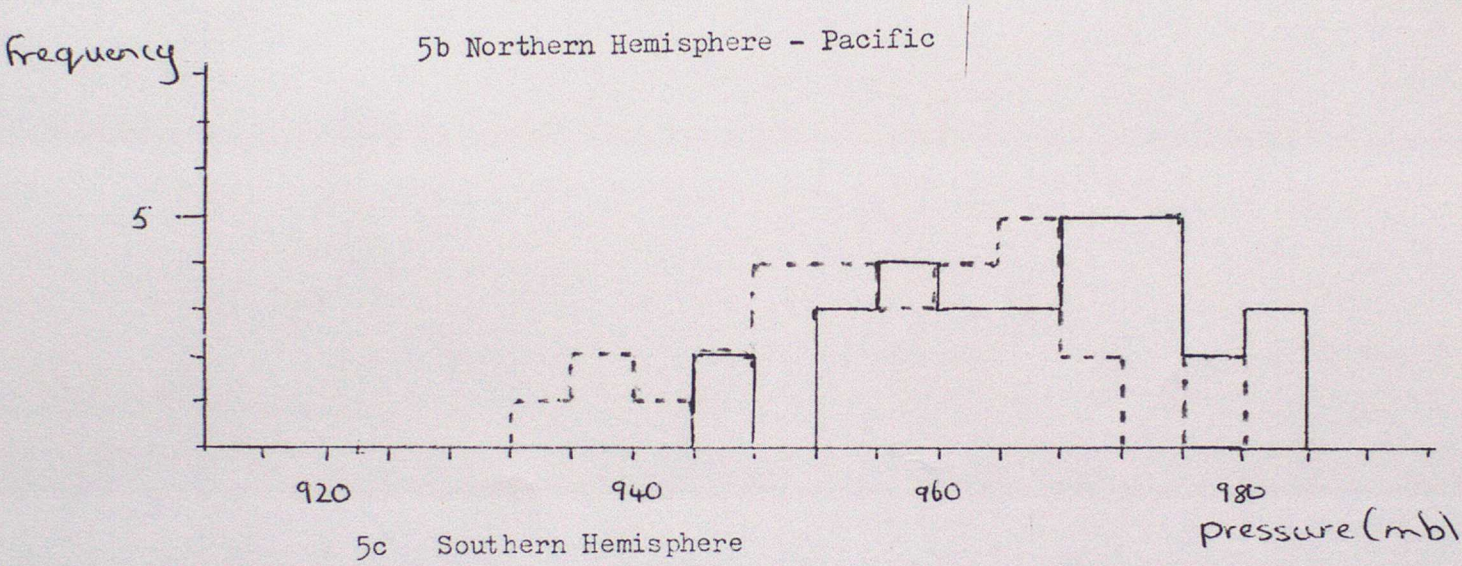

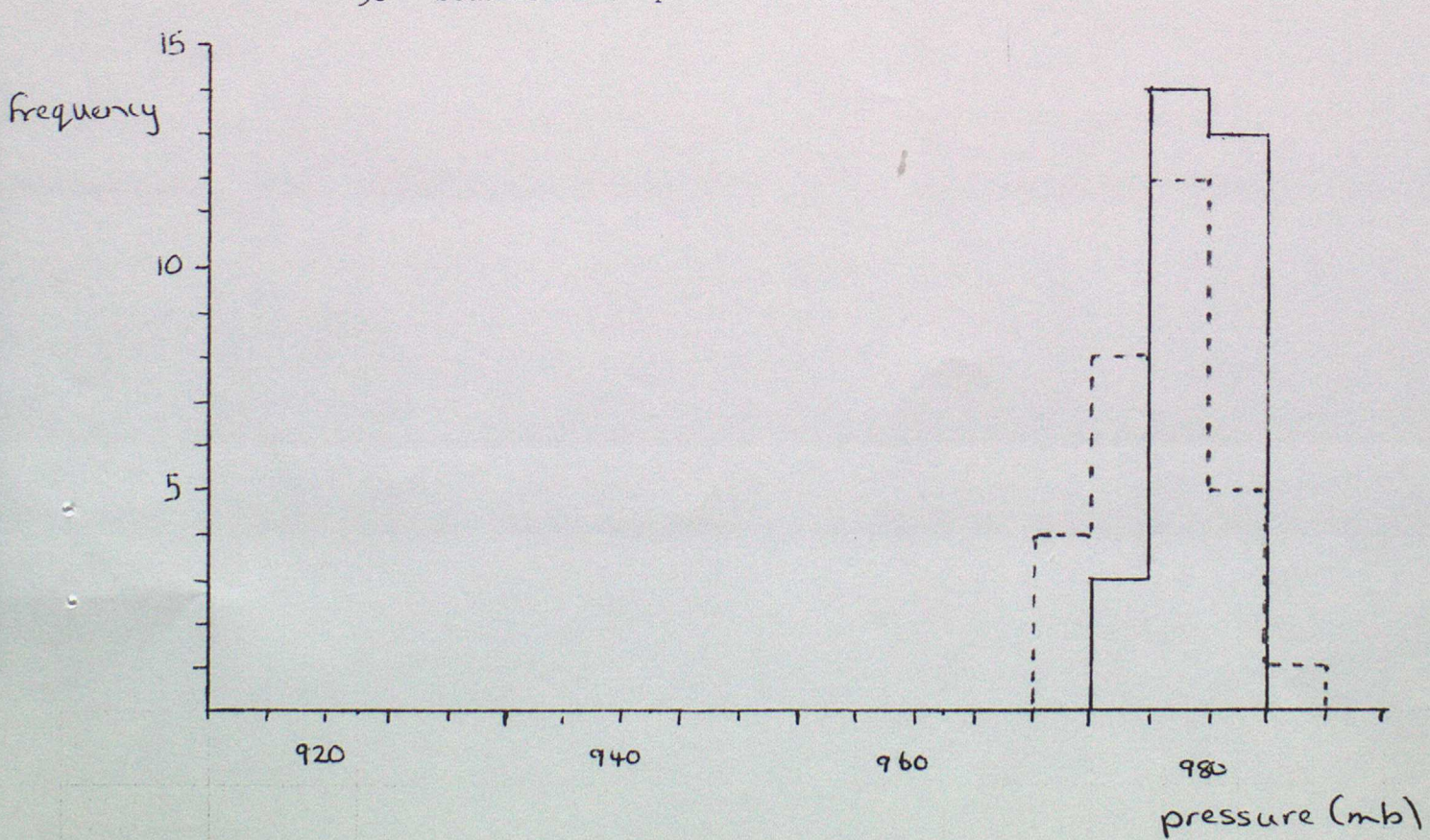

Figure 5: Histogram of occurrence of deepest low for days 51 to 80.

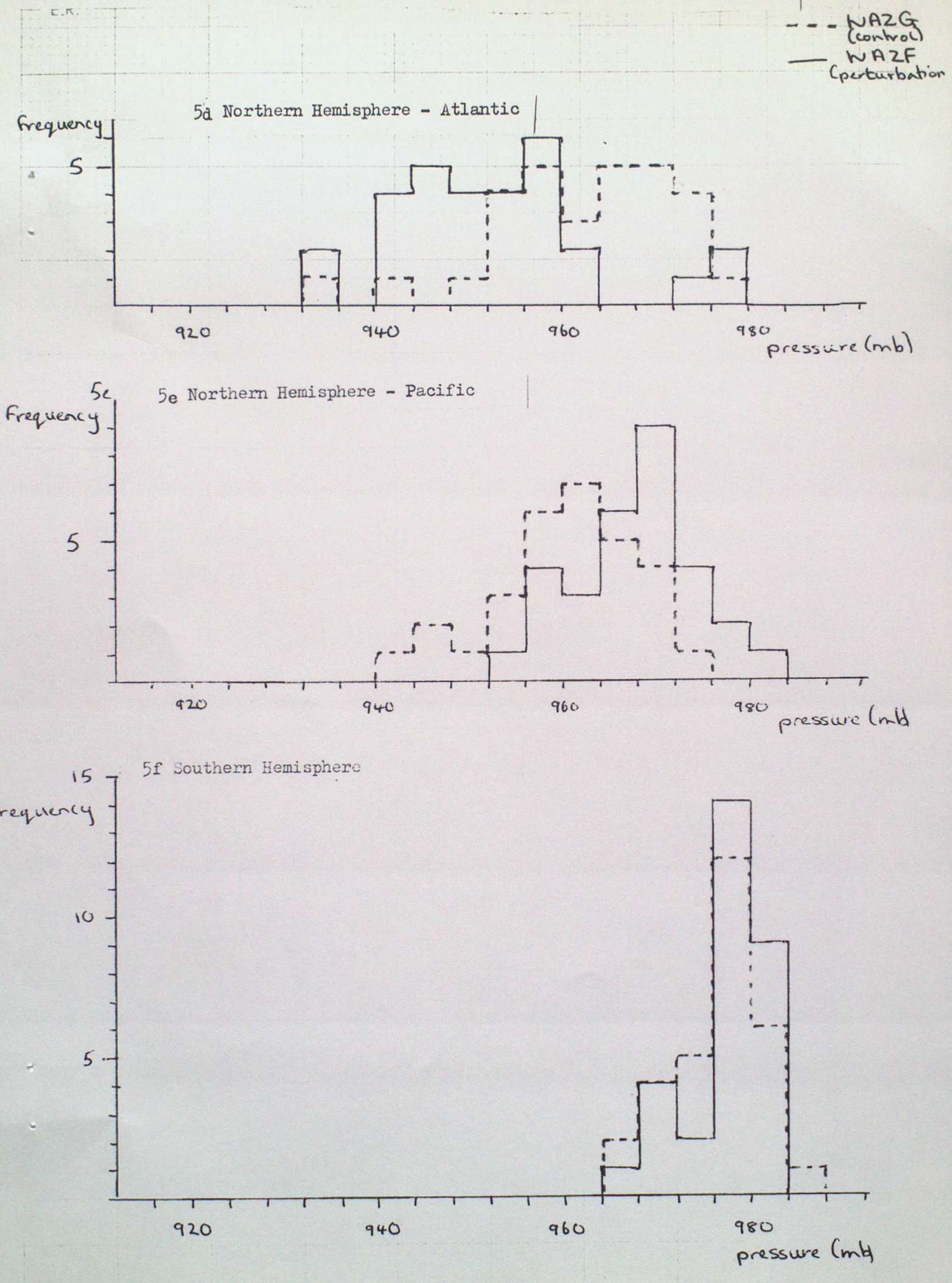

6a

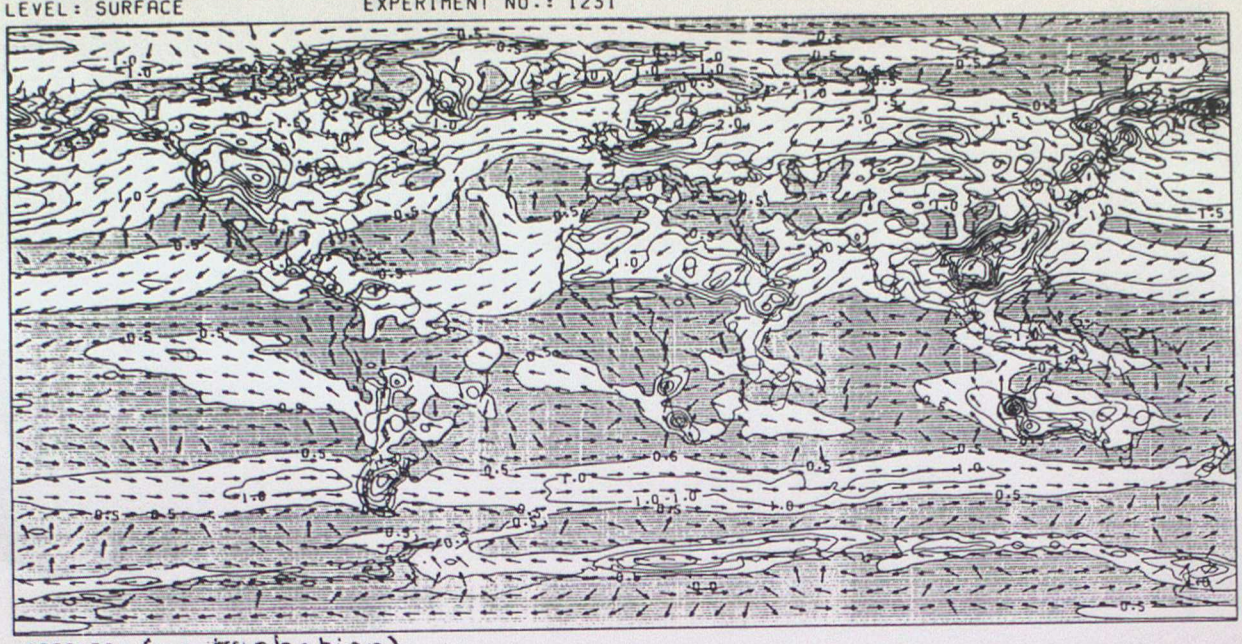

6b

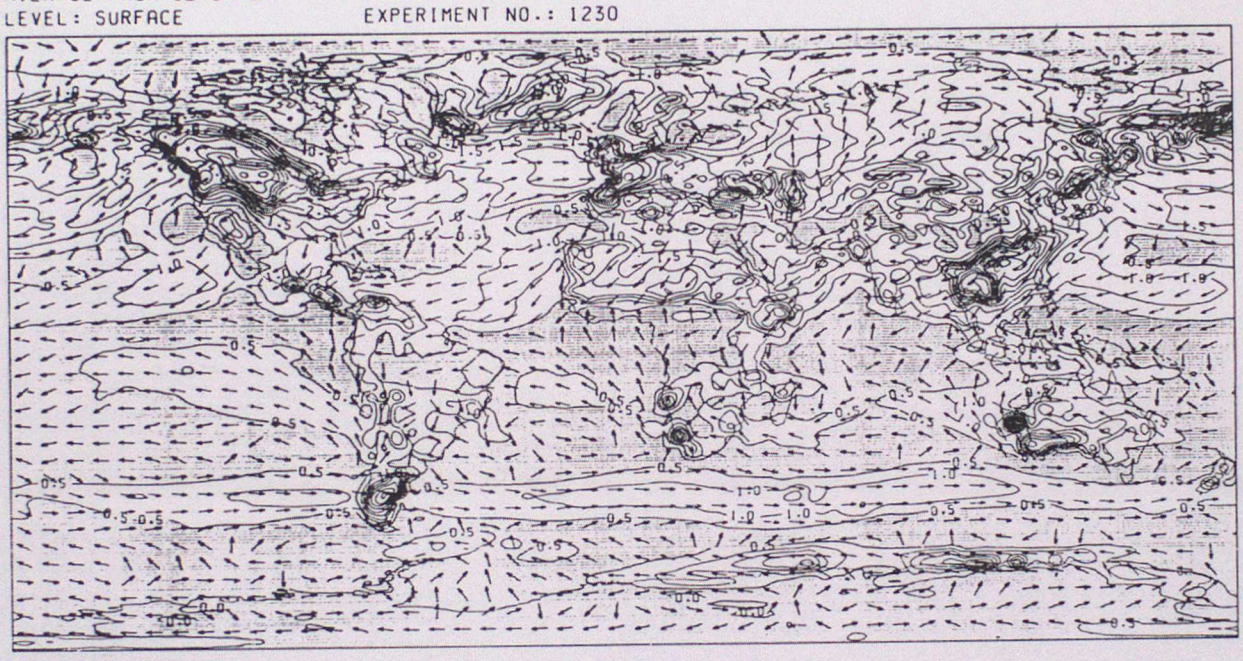

6c

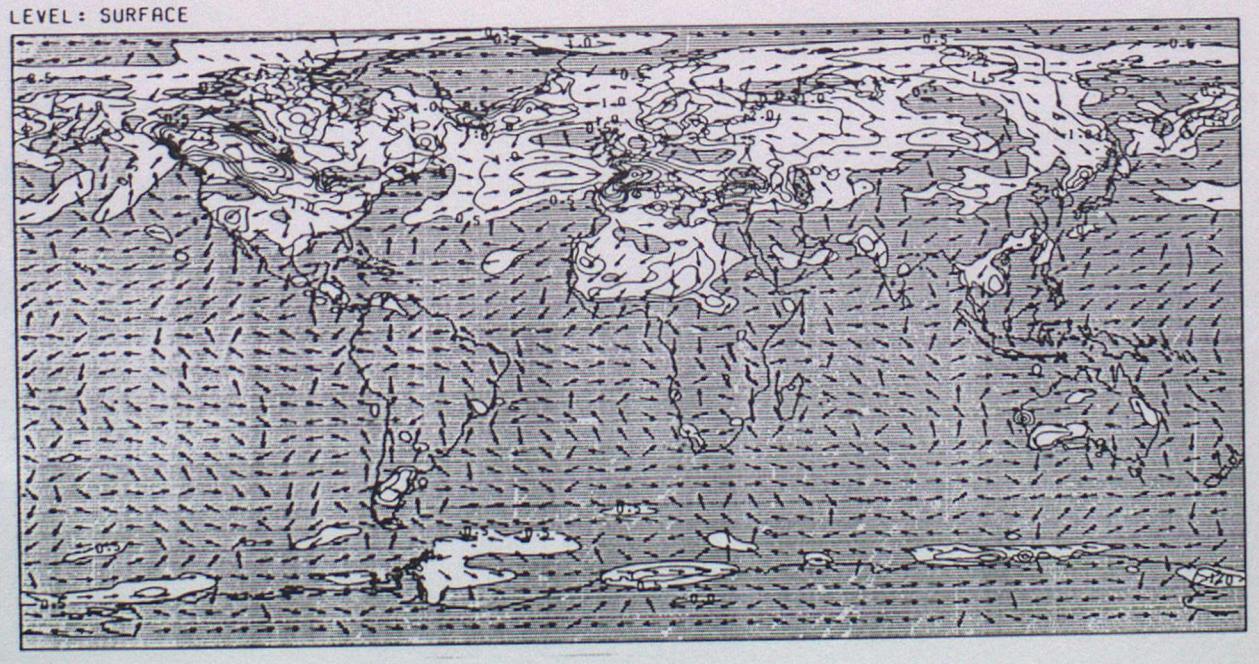

Figure 6: Surface stress in dynes/cm^2, a) WAZG2150, b) WAZF2150, c) WAZF2150 – WAZG2150

6d

SURFACE WIND STRESS DIAGNOSED
WAZG5180 (control)
AVERAGE FROM 0Z ON DAY 79 TO 0Z ON 1/0 DAY 80
LEVEL: SURFACE EXPERIMENT NO.: 1231

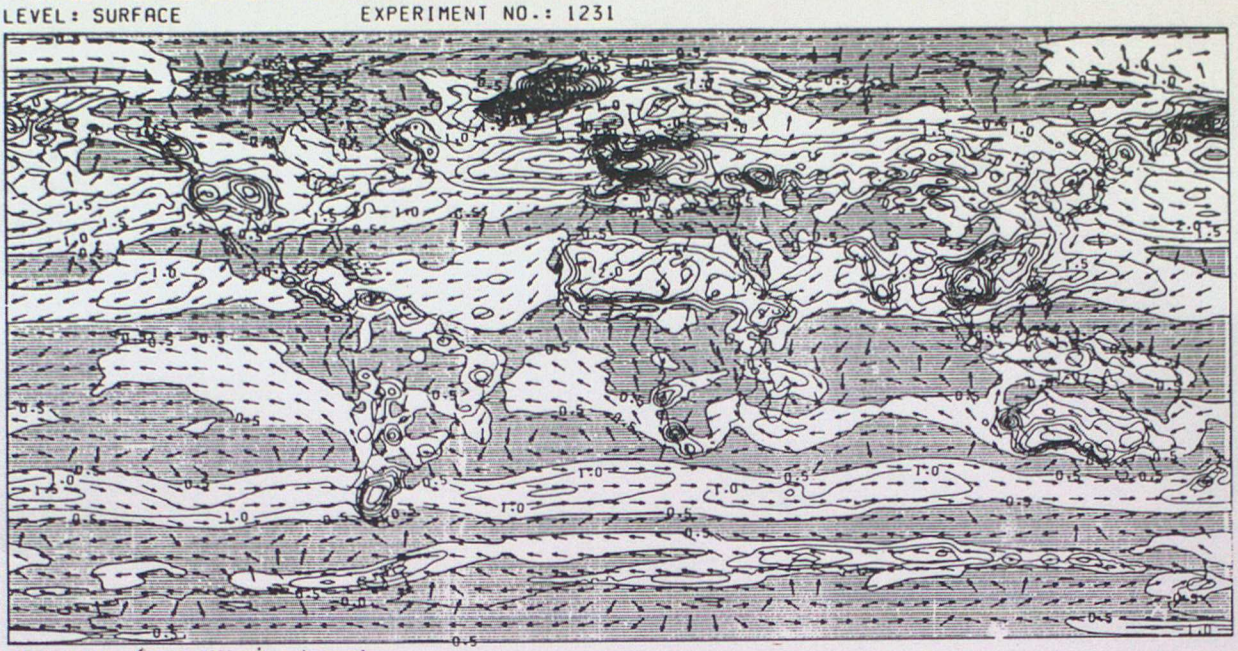

6e

WAZF5180 (perturbation)
AVERAGE FROM 0Z ON DAY 79 TO 0Z ON 1/0 DAY 80
LEVEL: SURFACE EXPERIMENT NO.: 1230

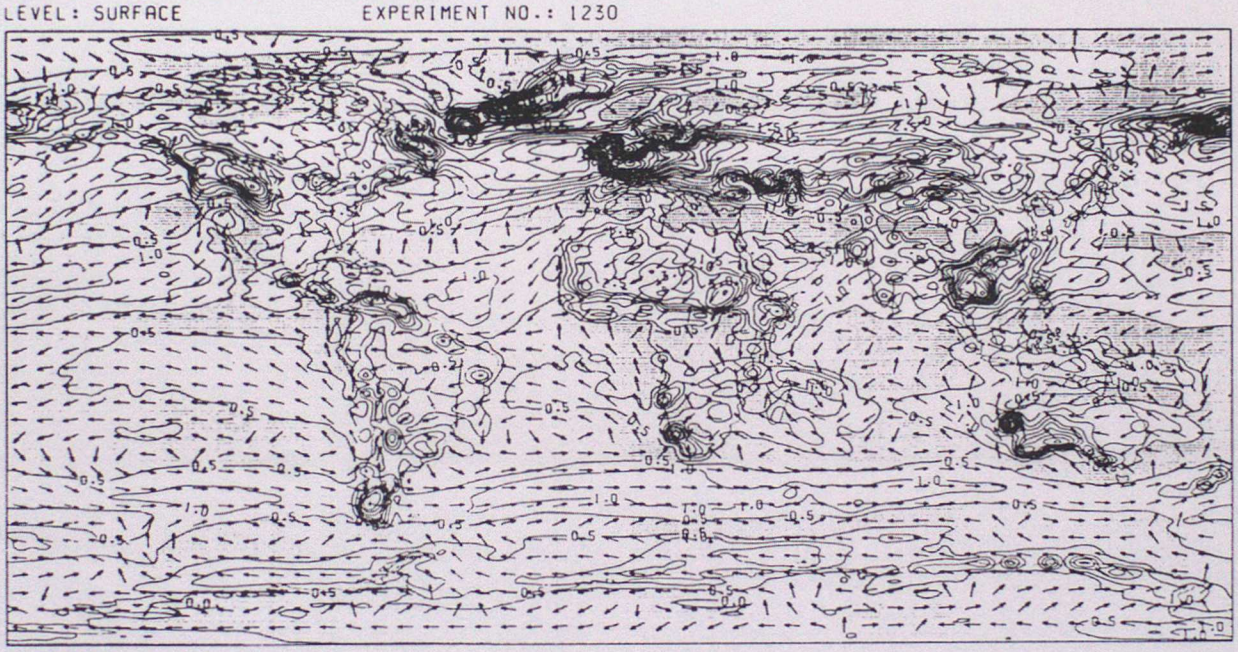

6f

WAZF5180 - WAZG5180
LEVEL: SURFACE

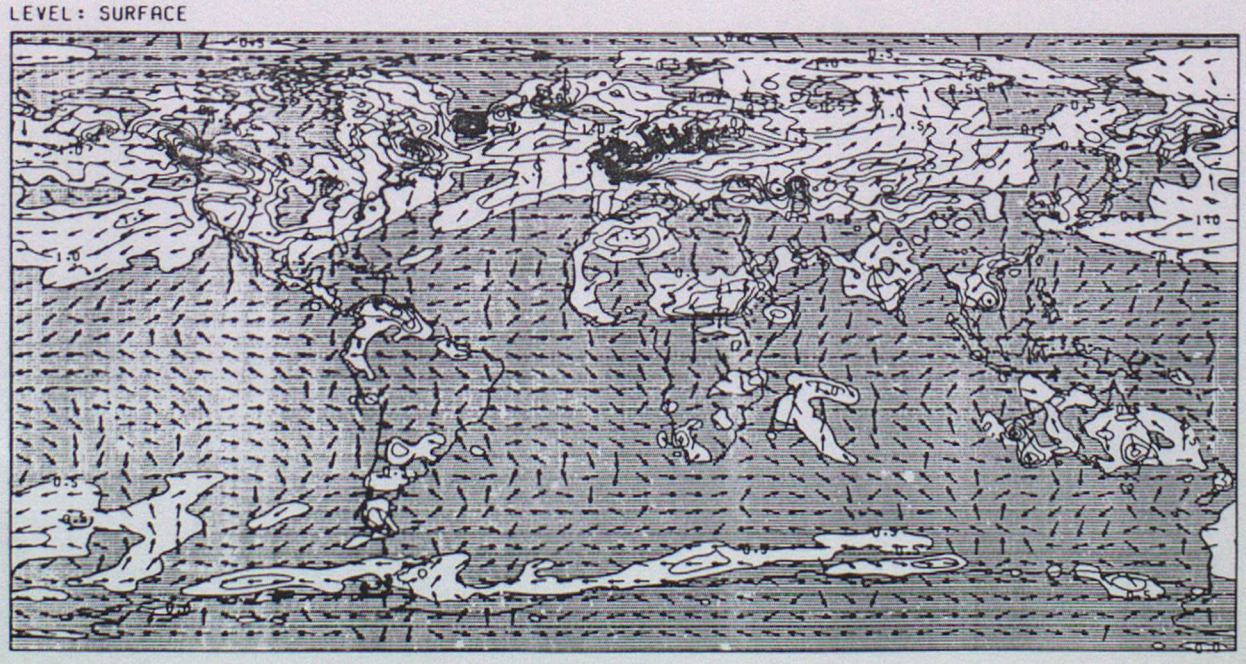

Figure 6: Surface stress in dynes/cm^2, d) WAZG5180, e) WAZF5180, f) WAZF5180 – WAZG5180

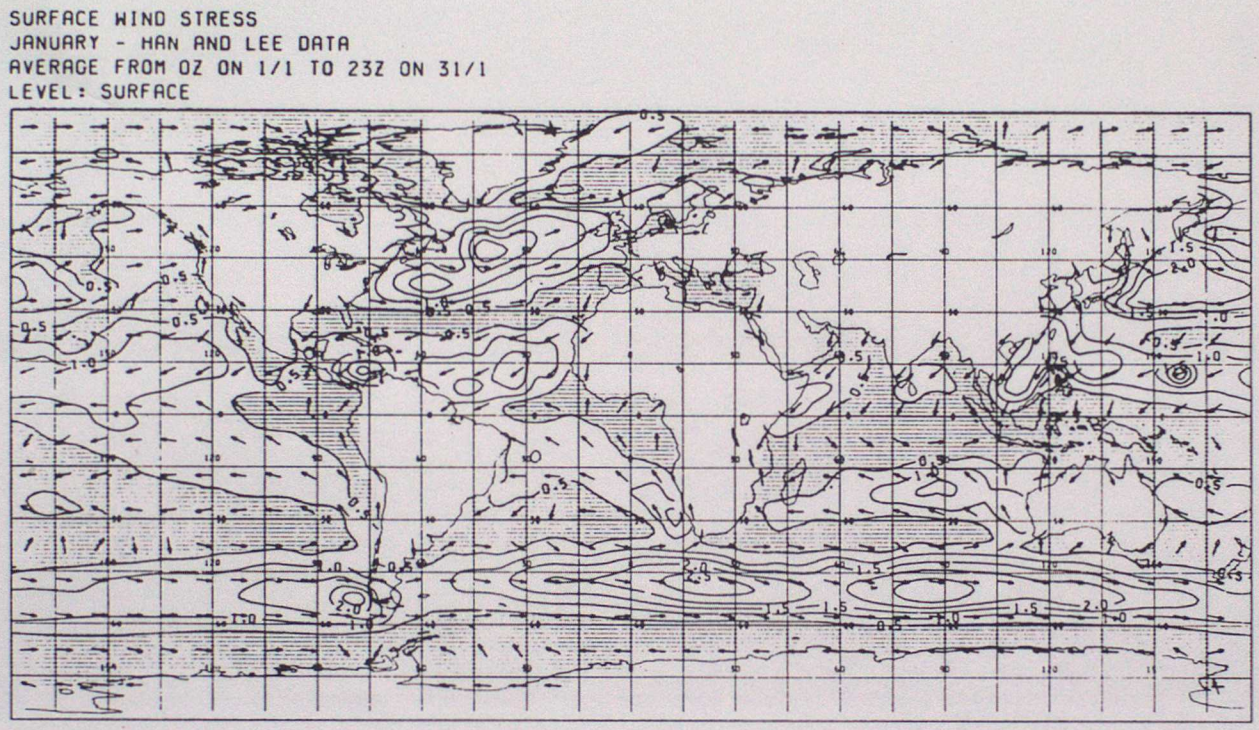

Figure 6: Surface stress in dynes/cm^2, g) Climatology (Han and Lee 1981).

Figure 7: Zonal mean zonal stress over land, a) days 21 to 50, b) days 51 to 80.

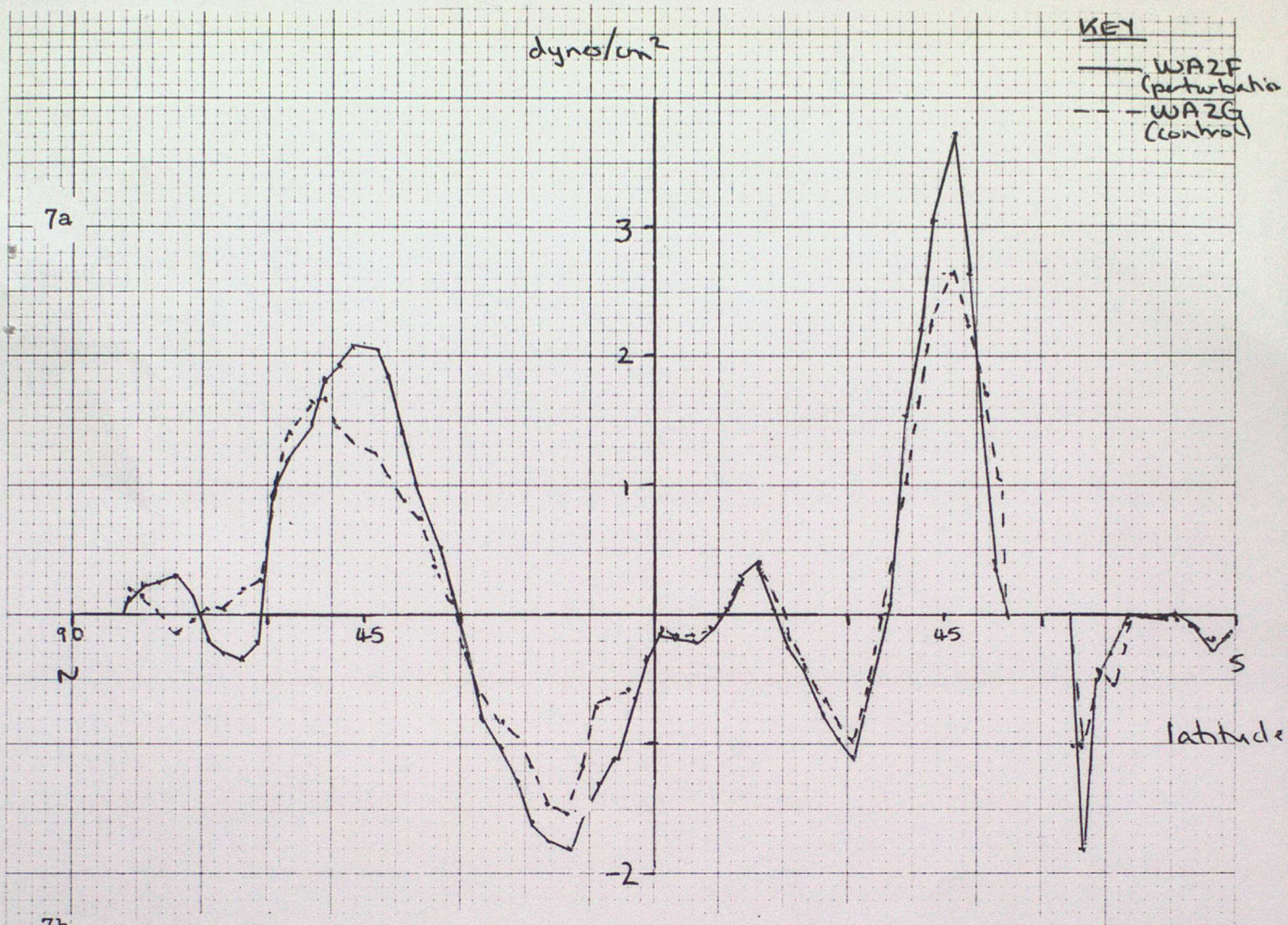

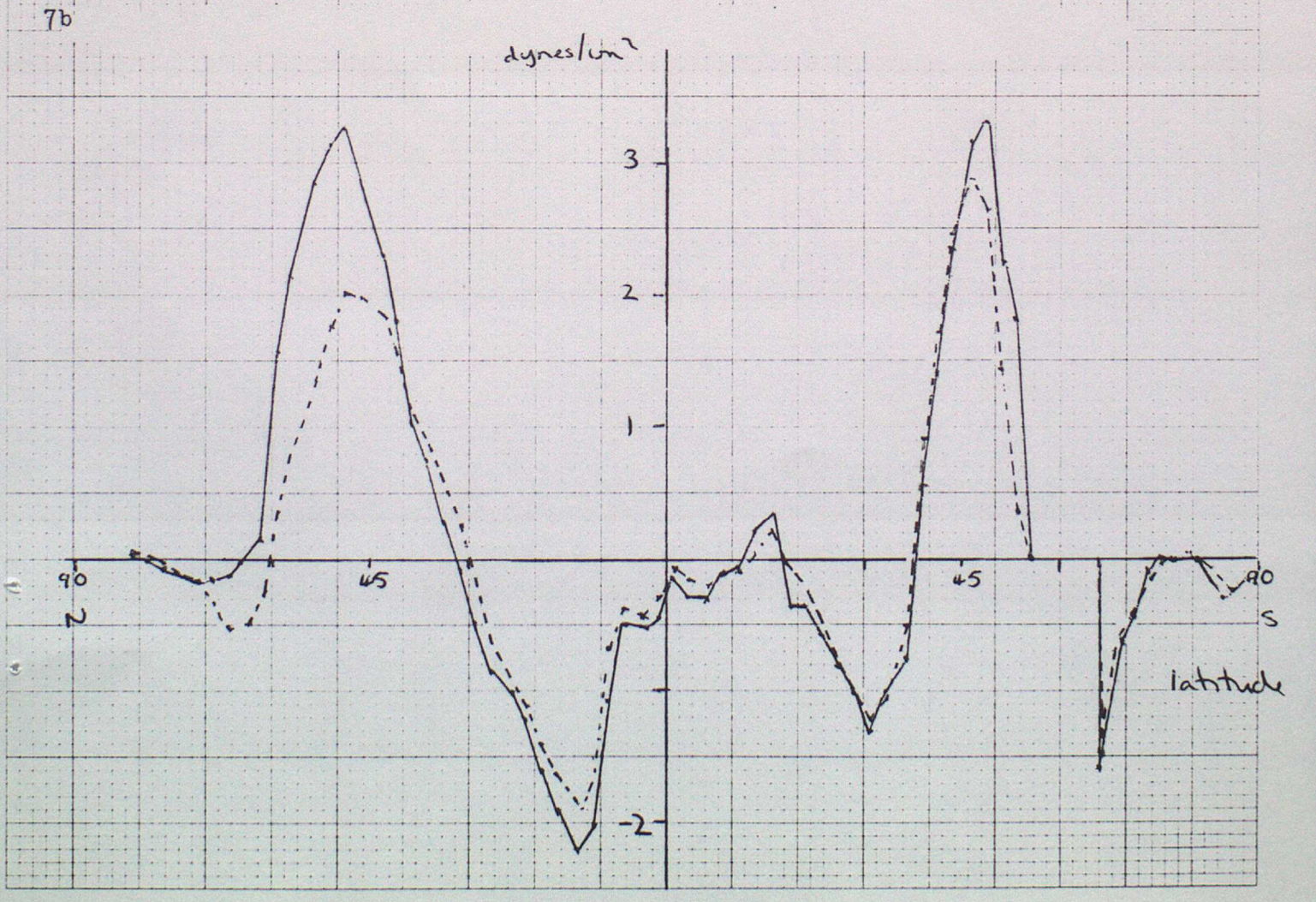

Figure 8: Zonal mean zonal stress over sea, a) days 21 to 50, b) days 51 to 80.

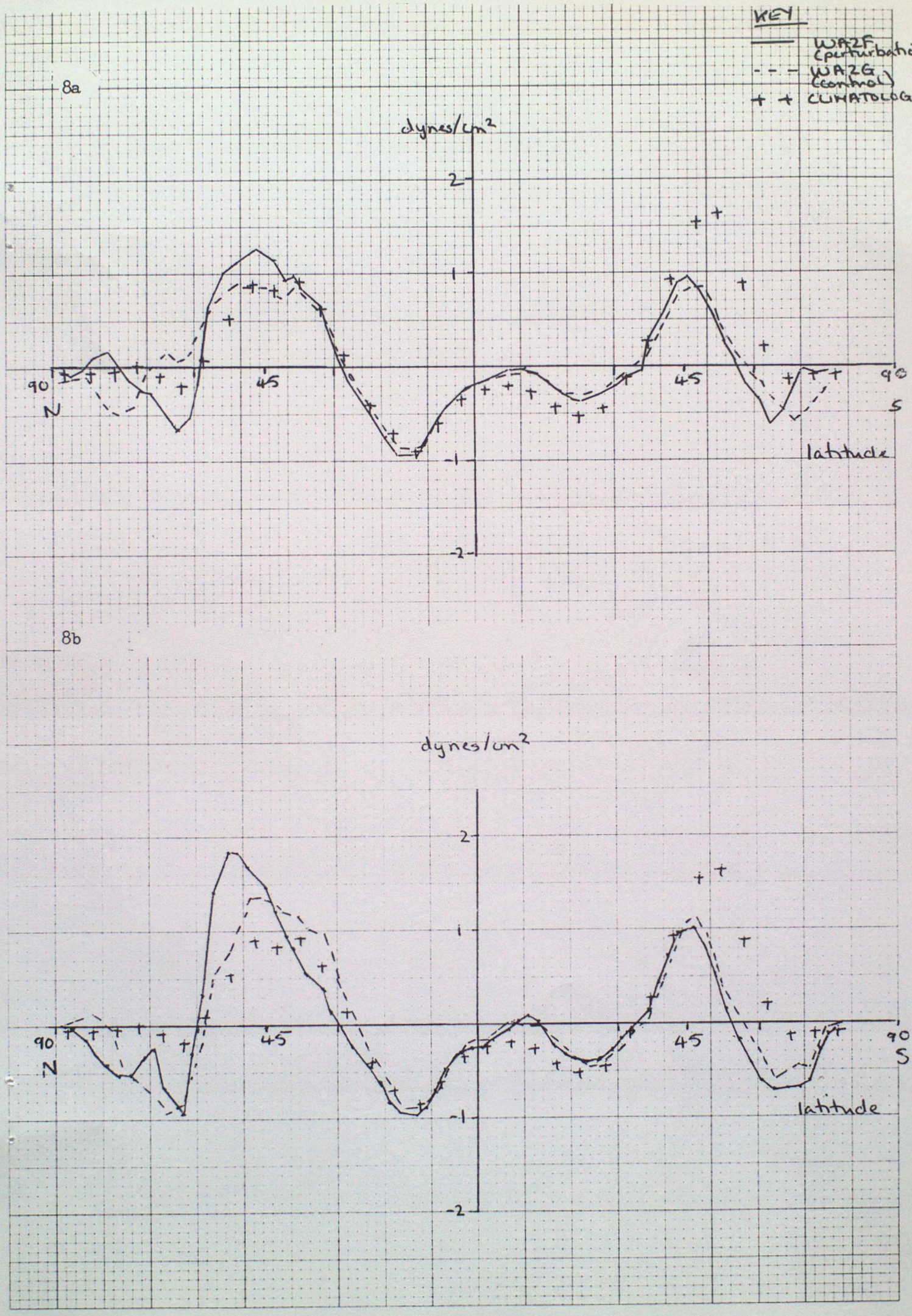

Figure 9 : Time series of global kinetic energy.

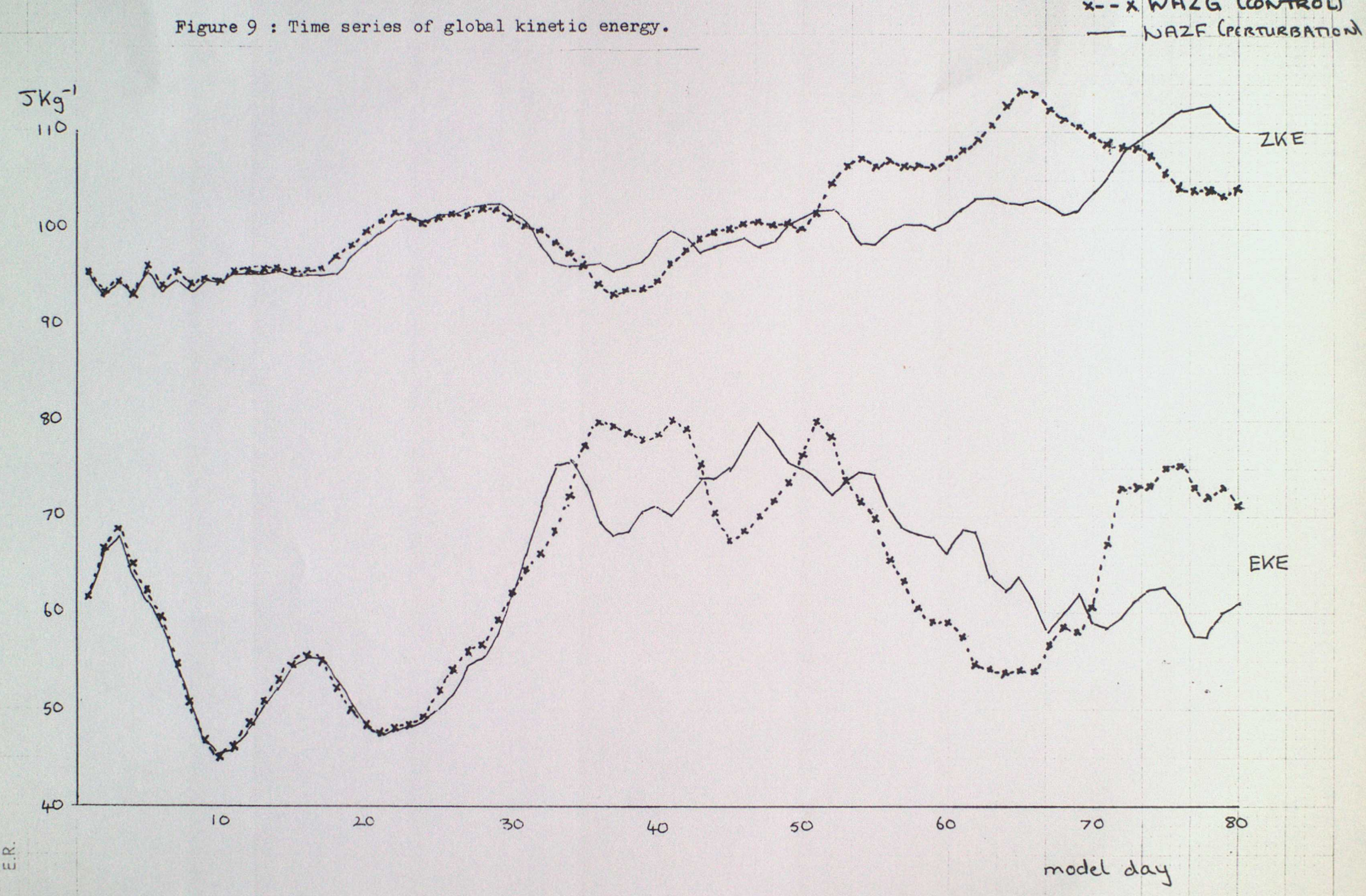

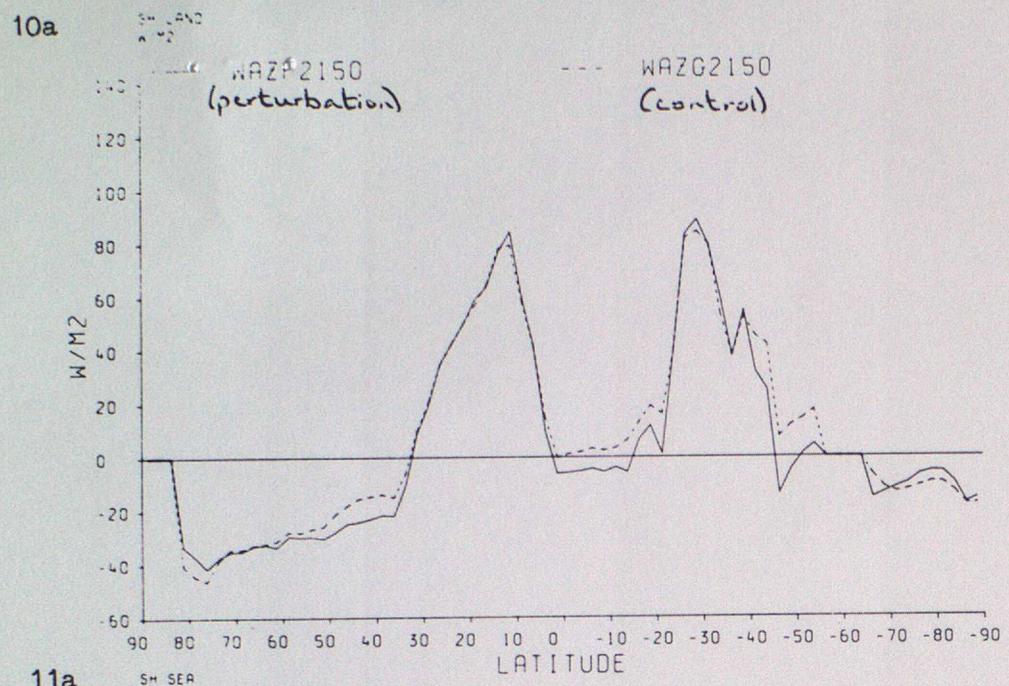

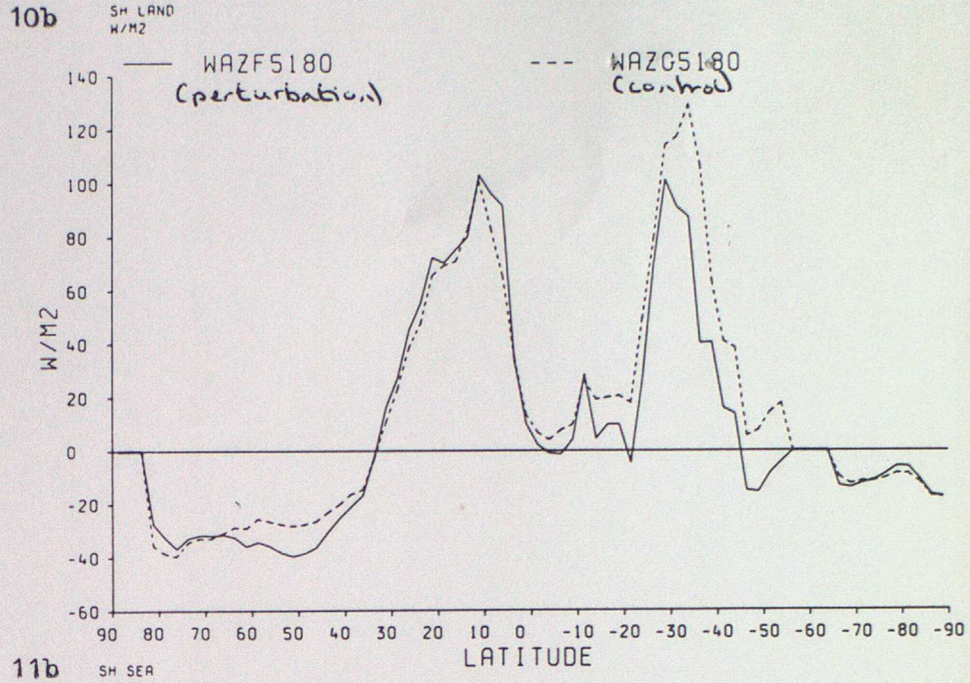

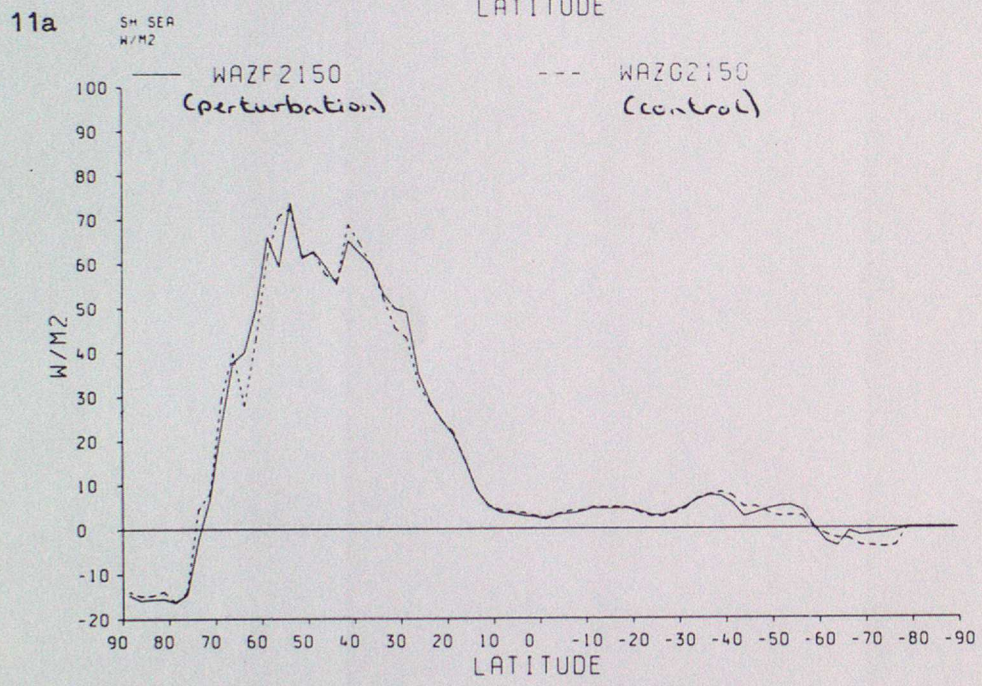

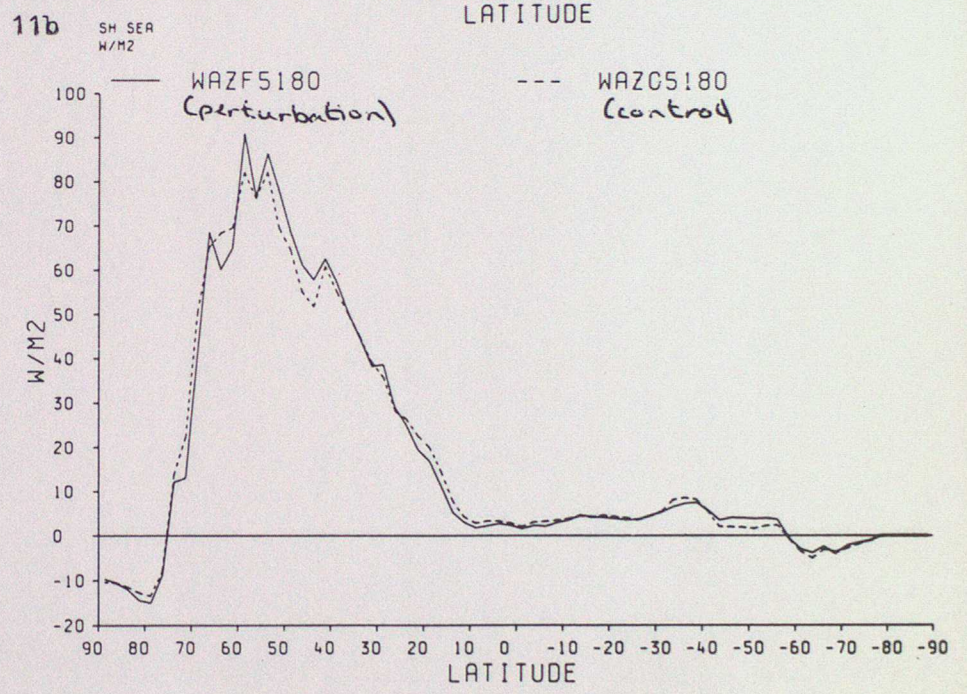

Figure 10: Zonal mean sensible heat flux from land and land-ice points

Figure 11: Zonal mean sensible heat flux from sea points.

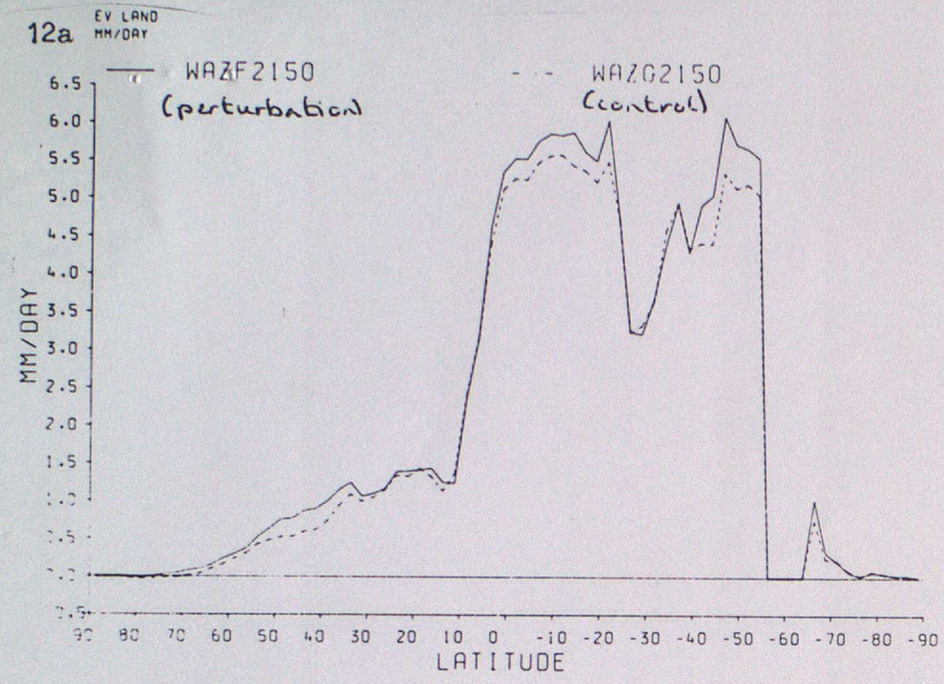

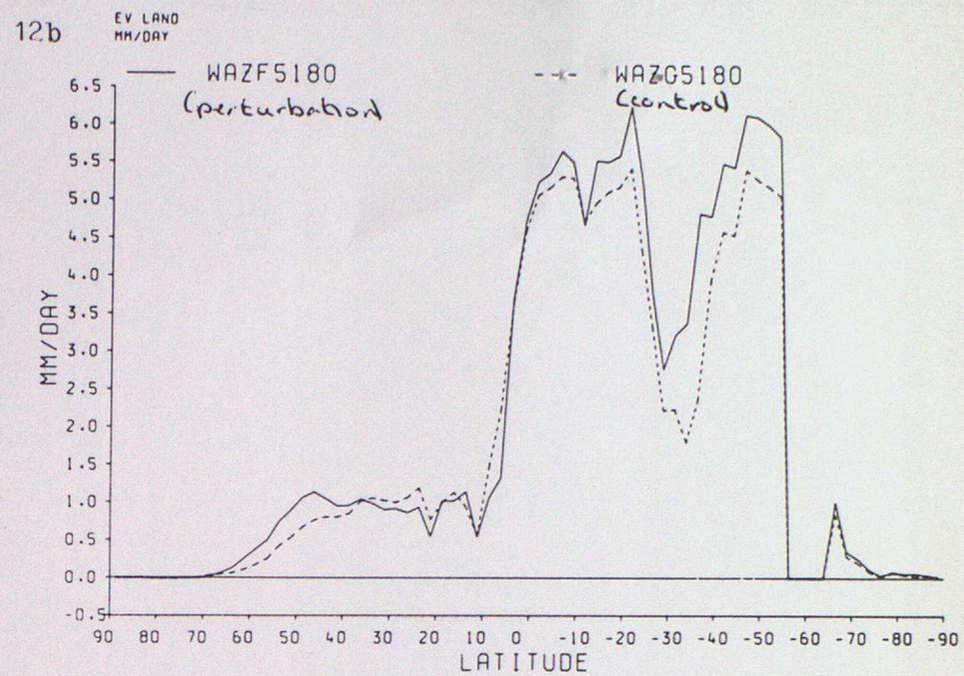

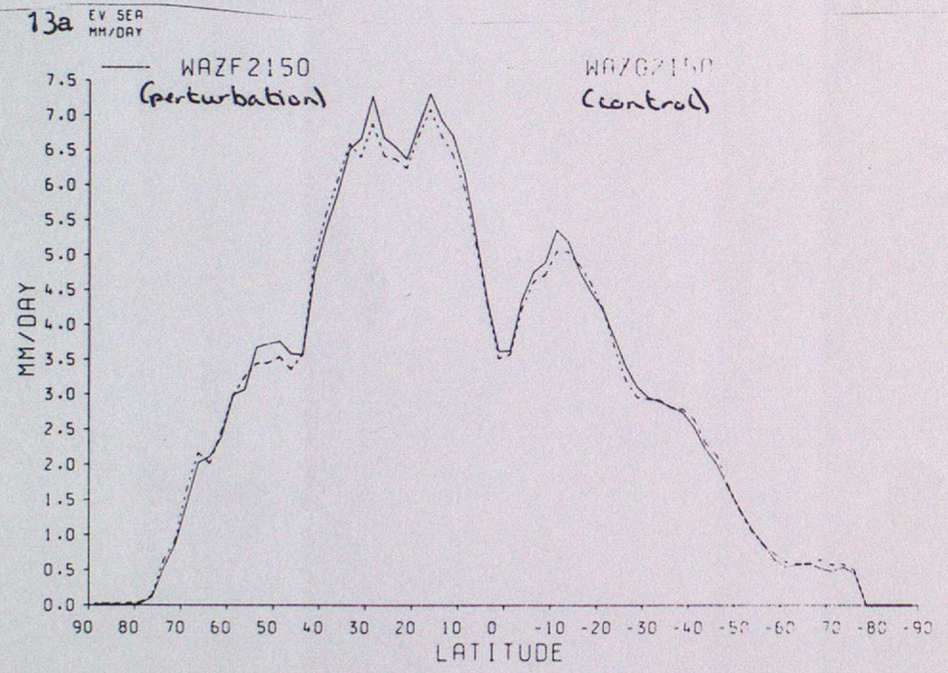

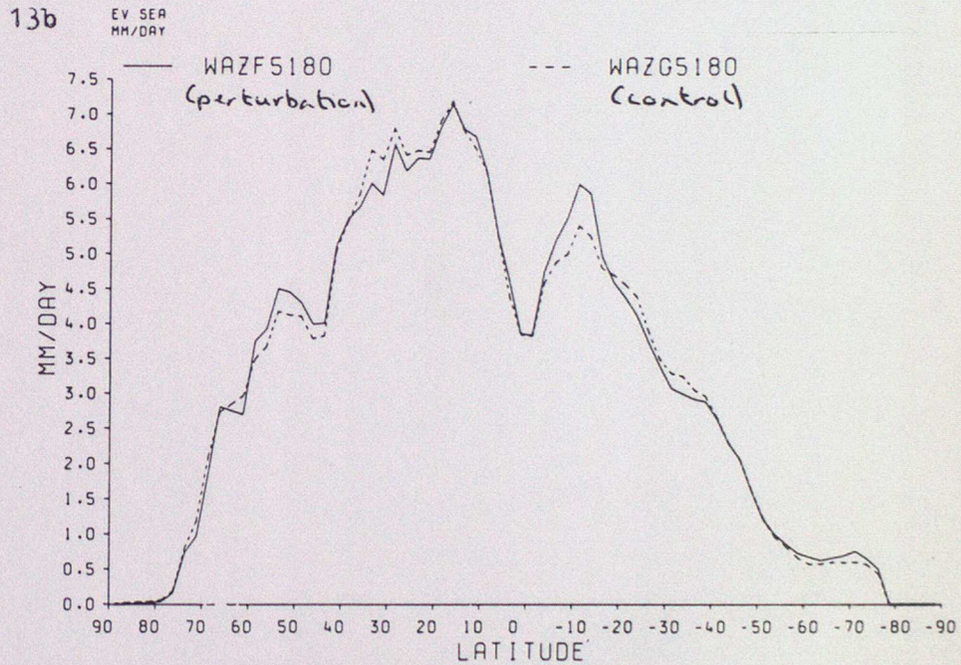

Figure 12 : Zonal mean evaporation from land and land-ice points.

Figure 13 : Zonal mean evaporation from sea points.

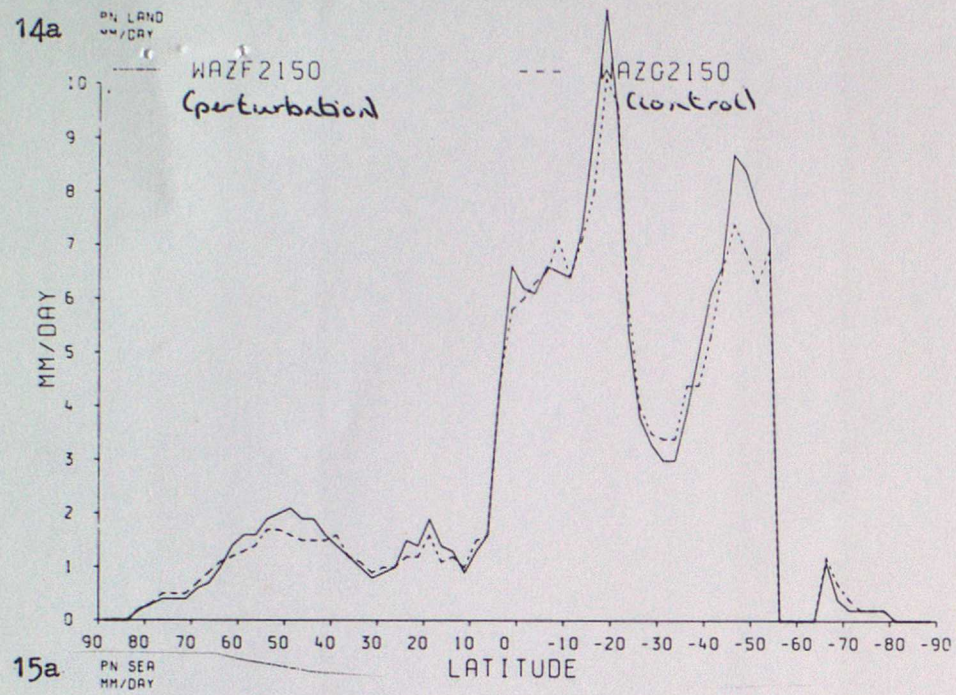

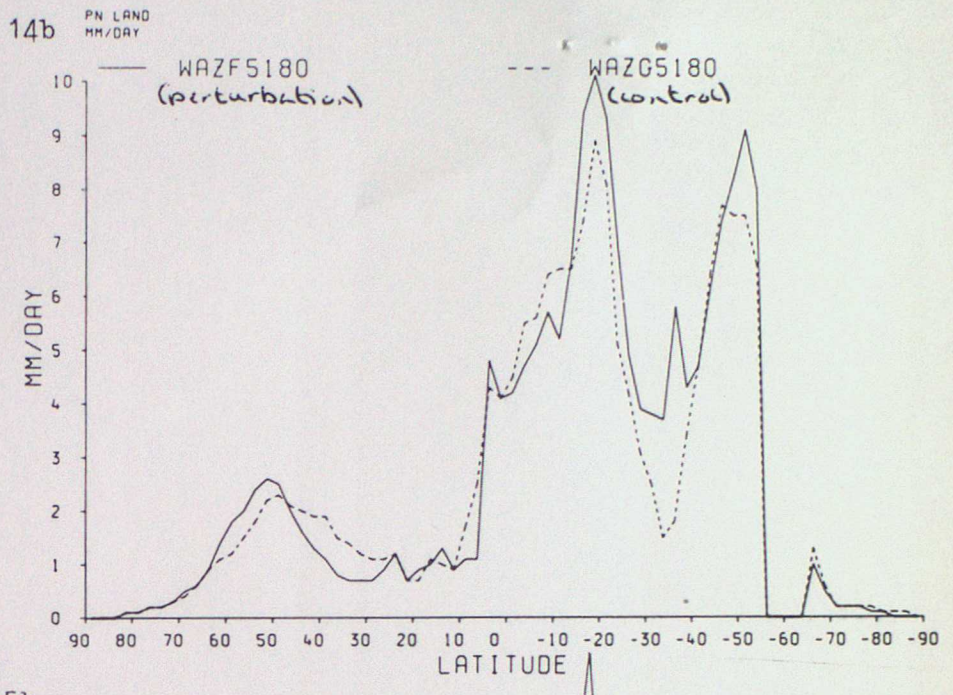

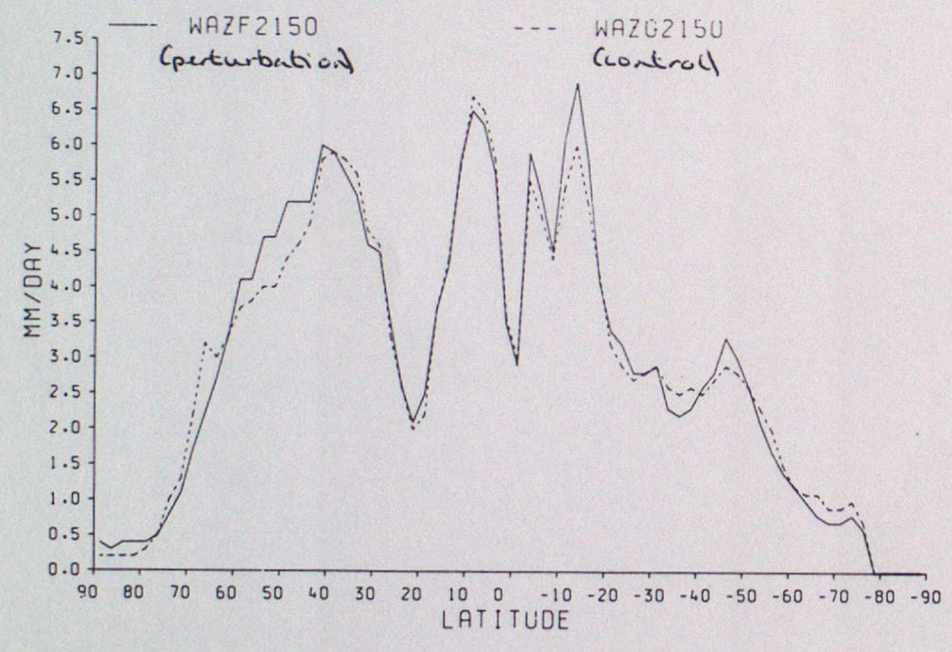

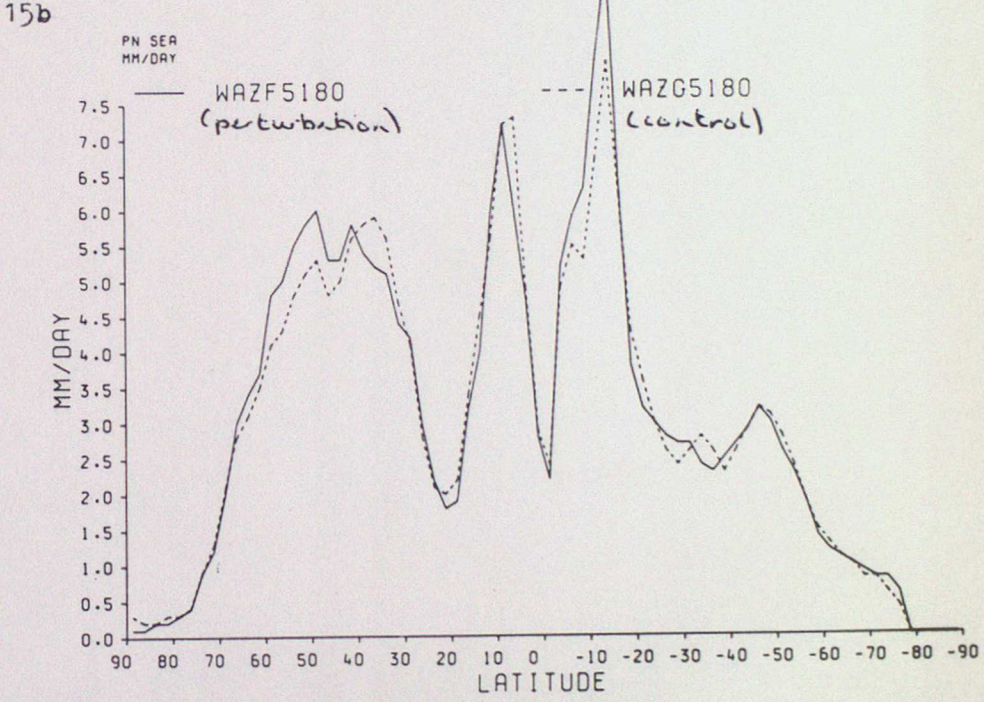

Figure 14: Zonal mean precipitation on land and land-ice points.

Figure 15: Zonal mean precipitation on sea points.

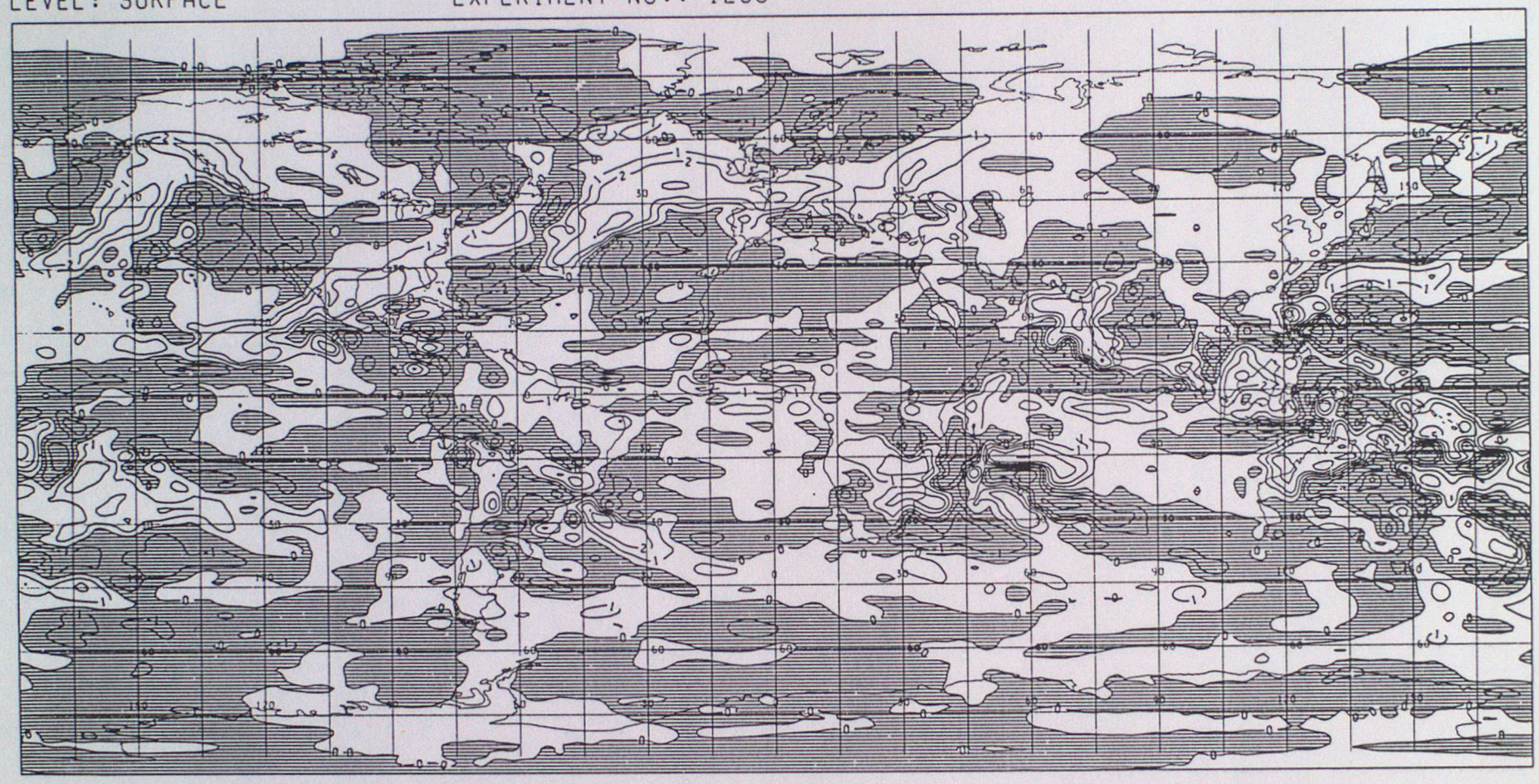

Figure 16: Precipitation differences in mm/day a) WAZF2150 -WAZG2150.

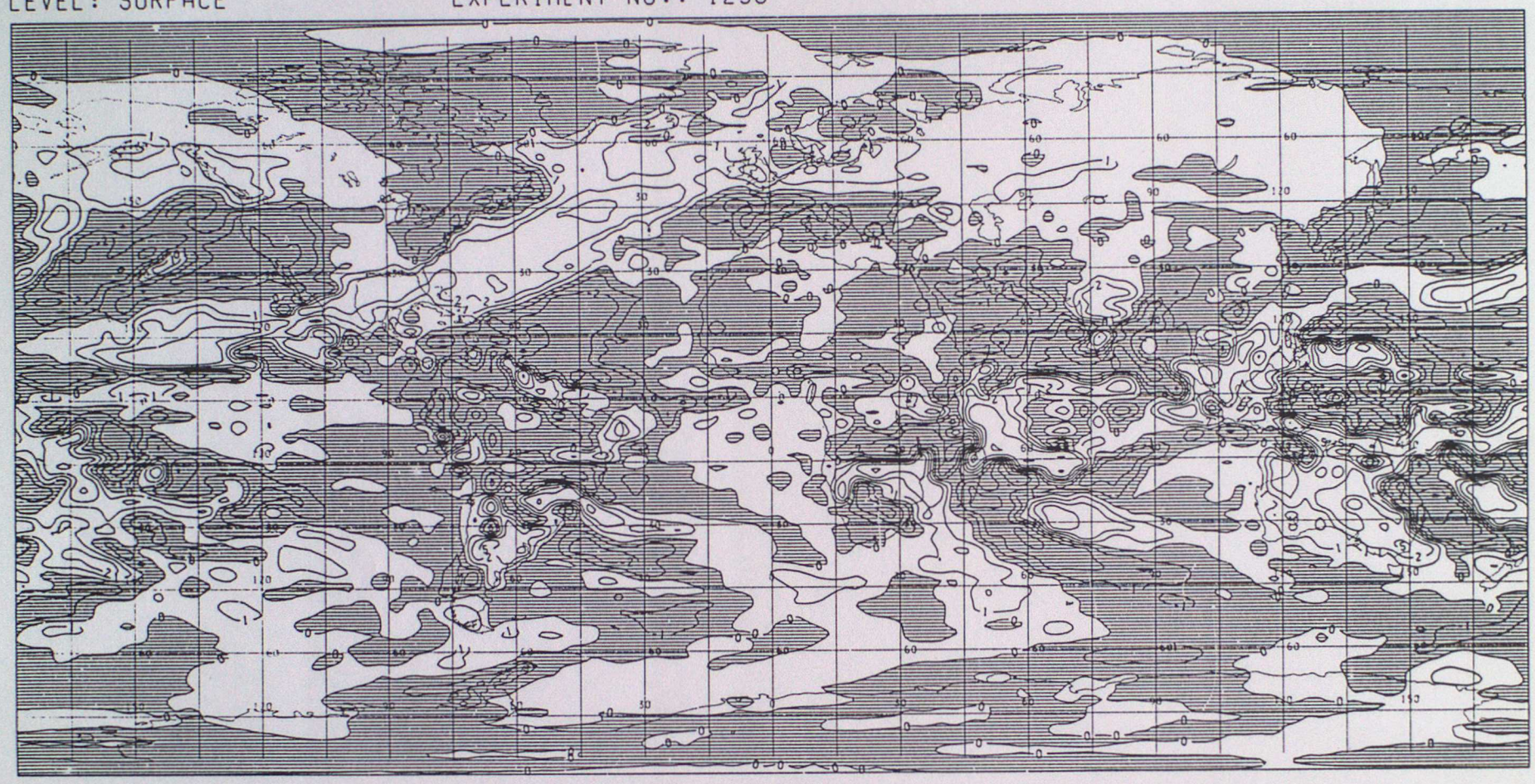

Figure 16: Precipitation differences in mm/day b) WAZF5180 - WAZG5180.

17a

PMSL.WAZG2150 (control)
AVERAGE FROM 0Z ON DAY 21 TO 0Z ON DAY 50
LEVEL: SEA LEVEL EXPERIMENT NO.: 1231

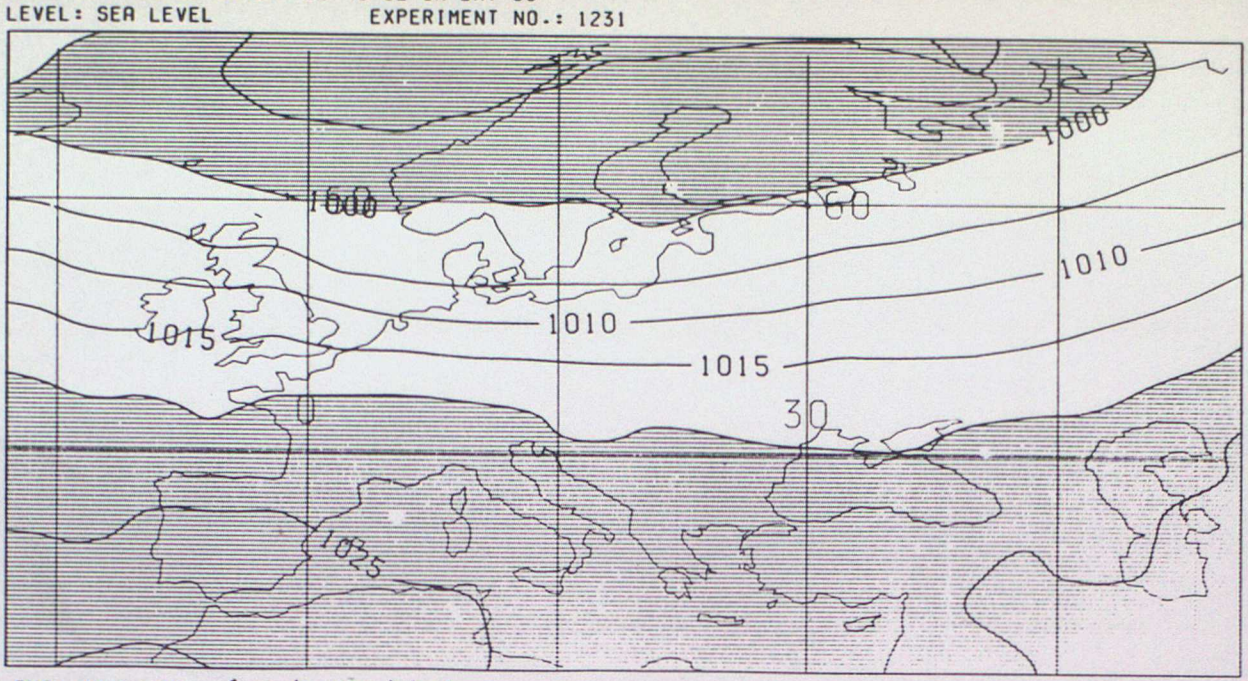

17b

PMSL.WAZF2150 (perturbation)
AVERAGE FROM 0Z ON DAY 21 TO 0Z ON DAY 50
LEVEL: SEA LEVEL EXPERIMENT NO.: 1230

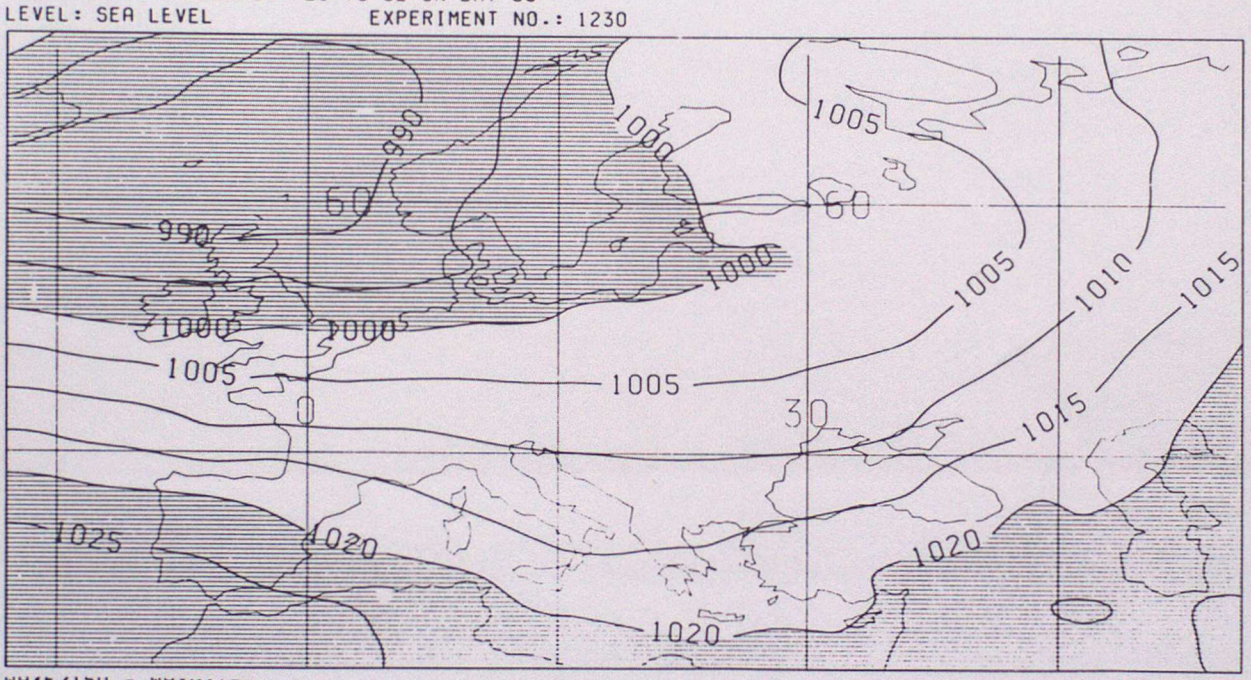

17c

WAZF2150 - WAZG2150
MEAN SEA LEVEL PRESSURE

LEVEL: SEA LEVEL

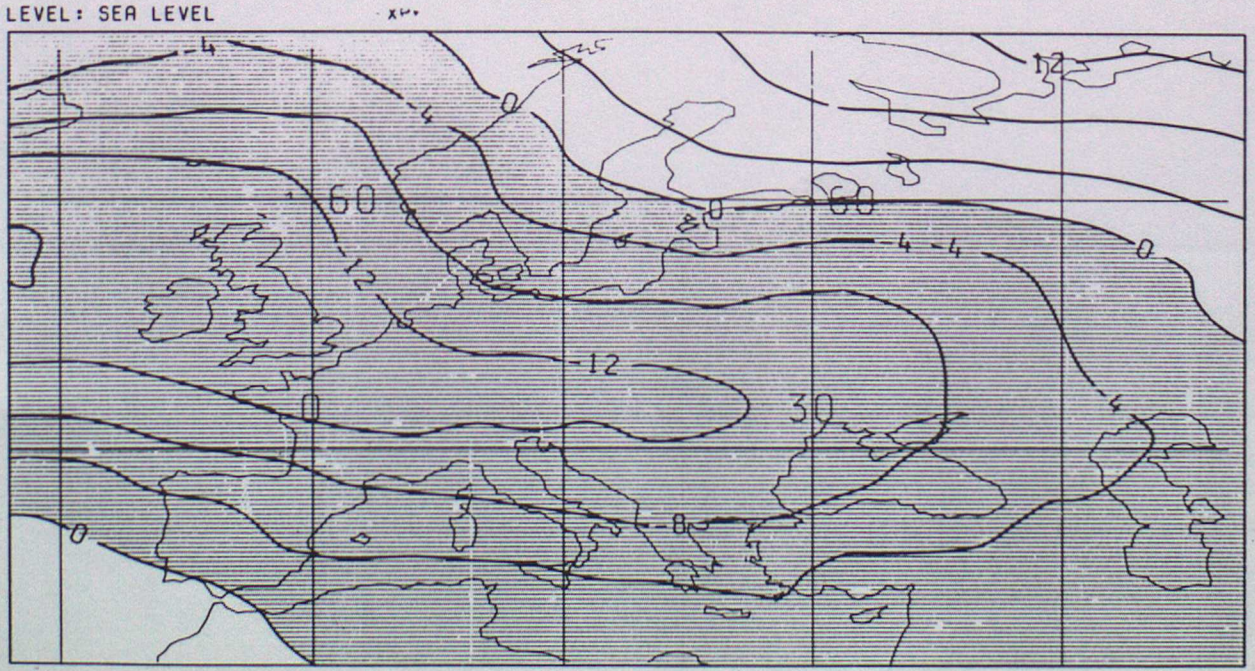

Figure 17: PMSL in European area, a) WAZG2150, b) WAZF2150, c) WAZF2150 – WAZG2150.

17d PMSL.WAZG5180 (control)
AVERAGE FROM 0Z ON DAY 51 TO 0Z ON DAY 80
LEVEL: SEA LEVEL EXPERIMENT NO.: 1231

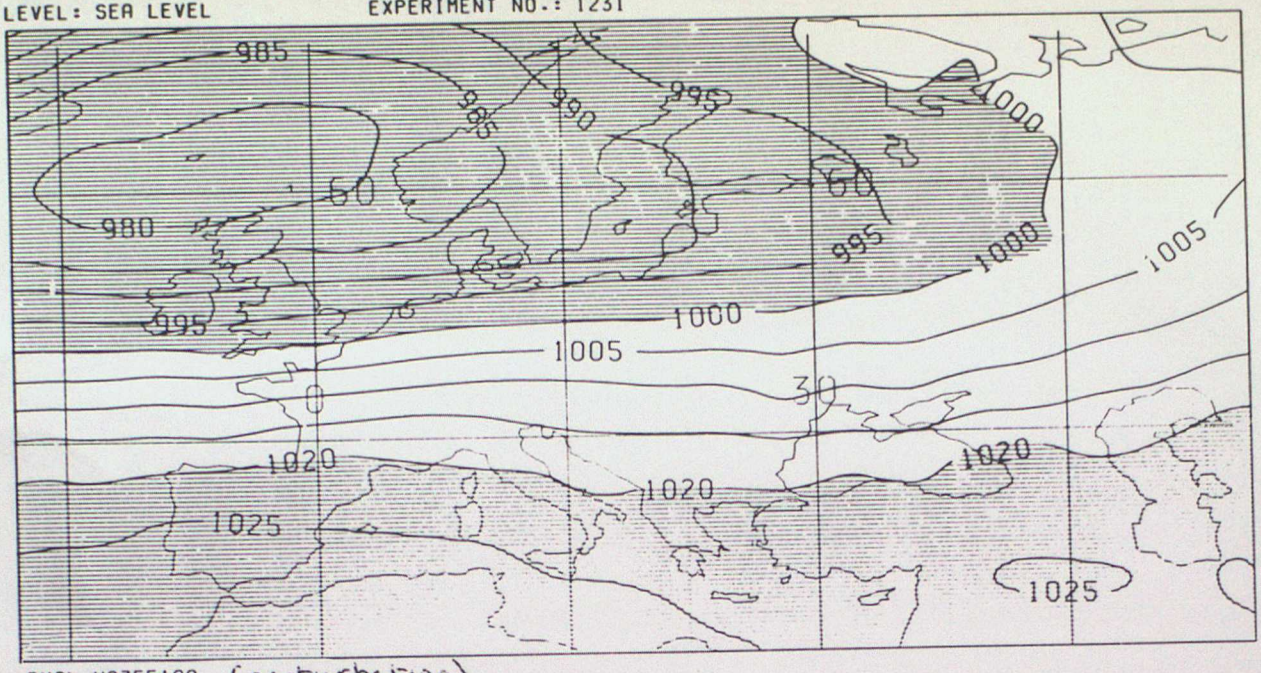

17e PMSL.WAZF5180 (perturbation)
AVERAGE FROM 0Z ON DAY 51 TO 0Z ON DAY 80
LEVEL: SEA LEVEL EXPERIMENT NO.: 1230

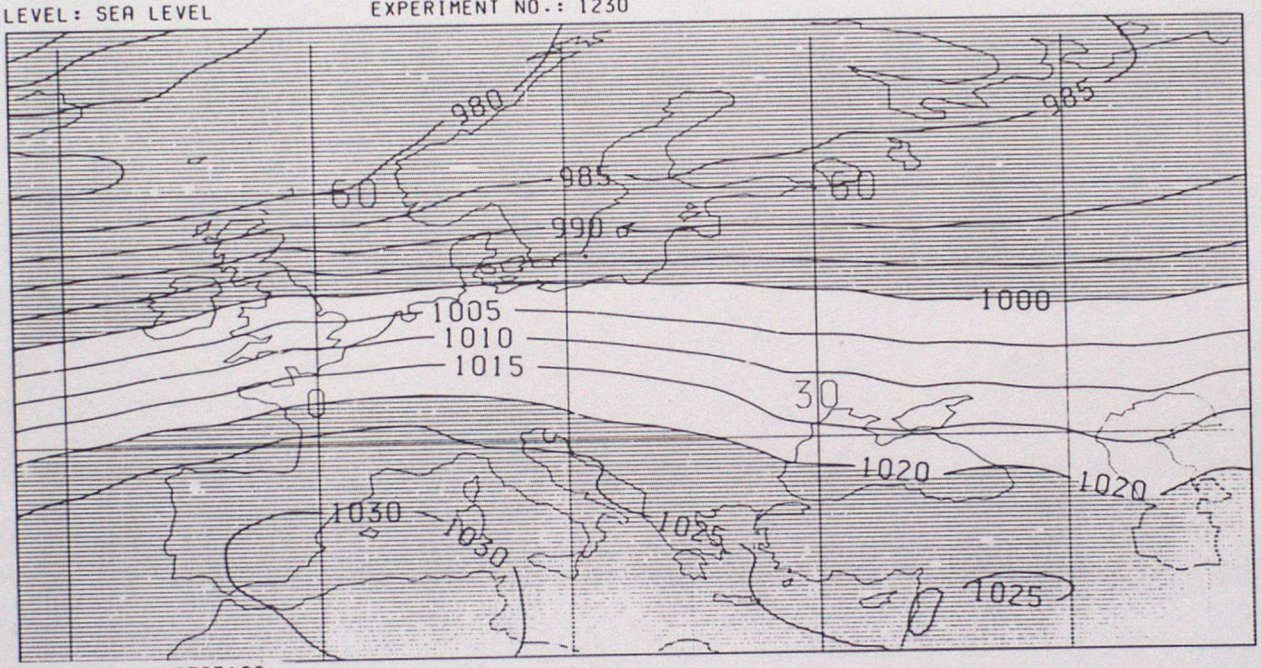

17f WAZF5180 - WAZG5180
MEAN SEA LEVEL PRESSURE
LEVEL: SEA LEVEL

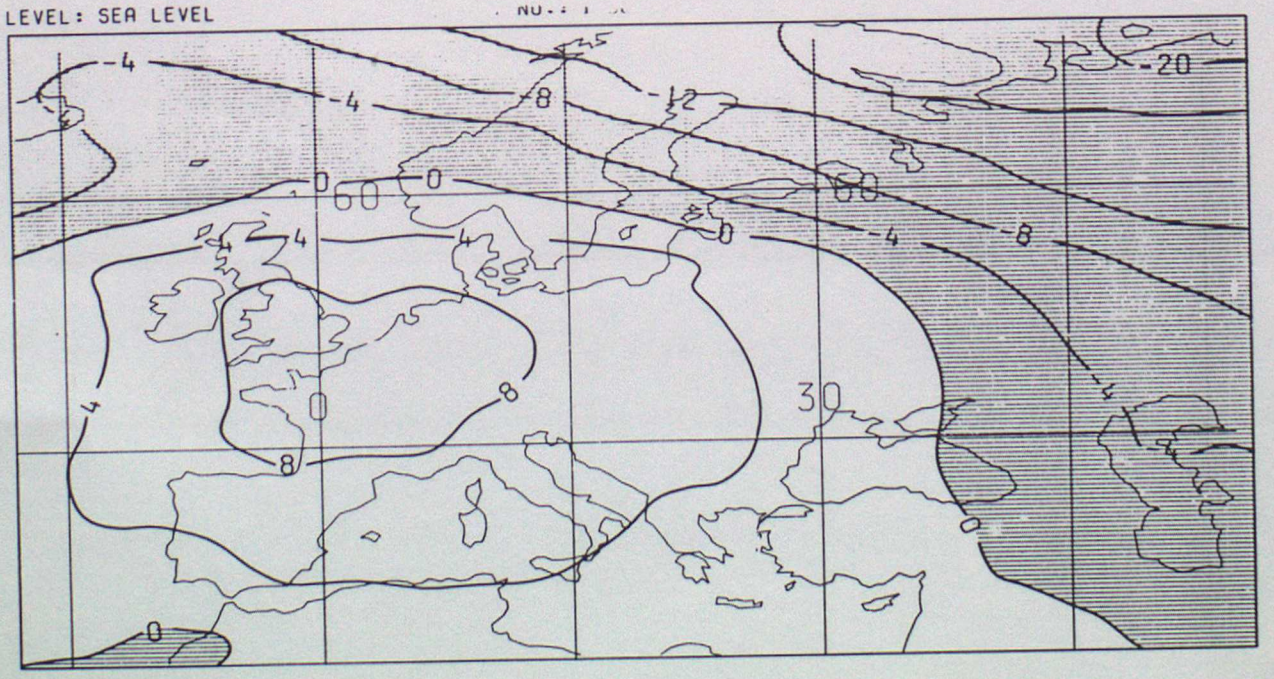

Figure 17: PMSL in European area, d) WAZG5180, e) WAZF5180, f) WAZF5180 - WAZG5180.

17g

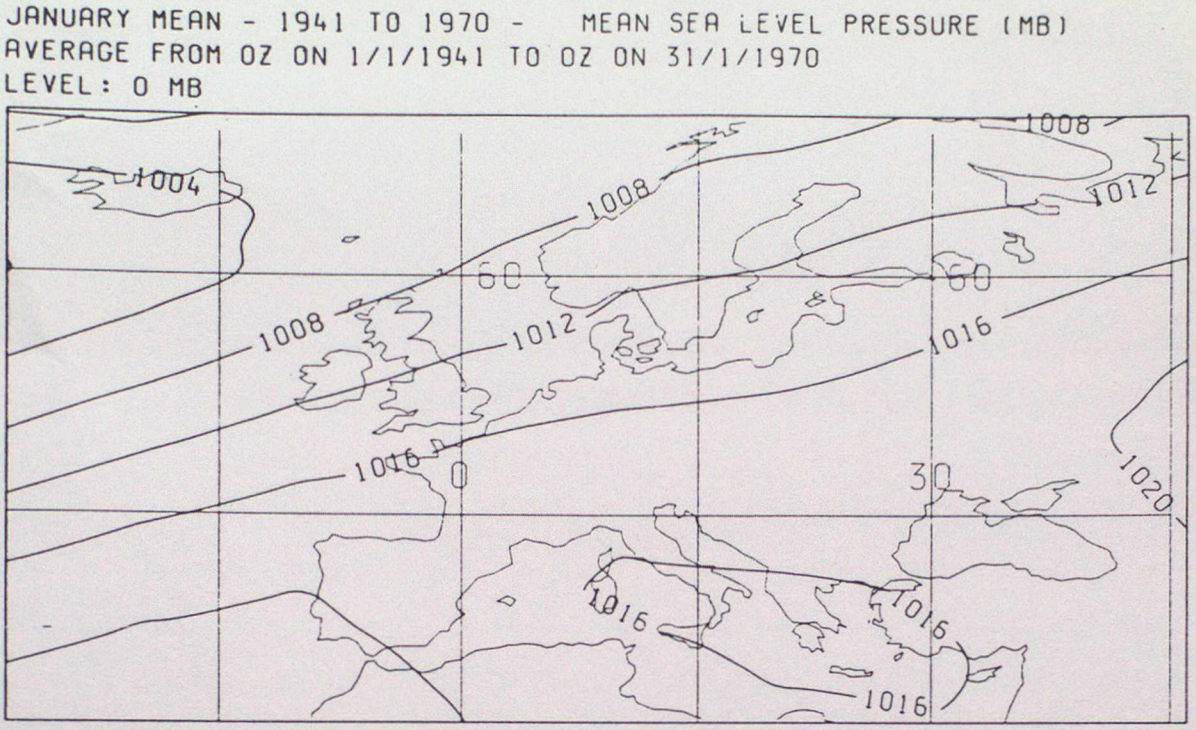

Figure 17: PMSL in European area, g) Climatology (Benwell 1982).

18a

PRECIPITATION. WAZG2150 (control)
AVERAGE FROM 0Z ON 2/12 DAY 21 TO 0Z ON 1/1/1 DAY 50
LEVEL: SURFACE EXPERIMENT NO.: 1231

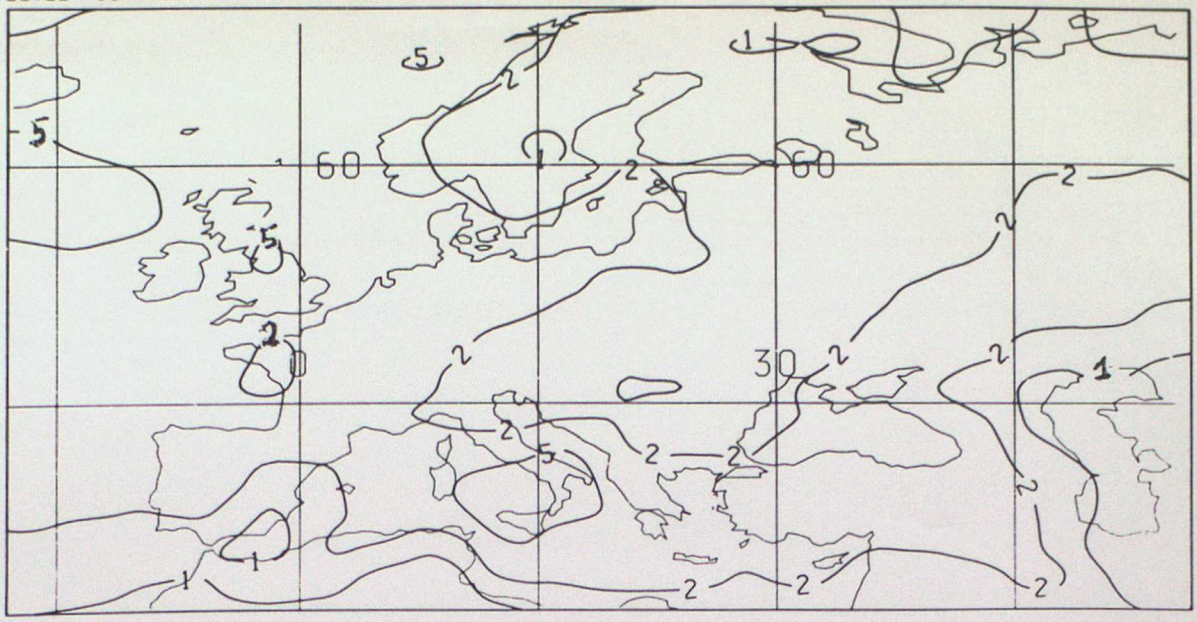

18b

PRECIPITATION. WAZF2150 (perturbation)
AVERAGE FROM 0Z ON 2/12 DAY 21 TO 0Z ON 1/1/1 DAY 50
LEVEL: SURFACE EXPERIMENT NO.: 1230

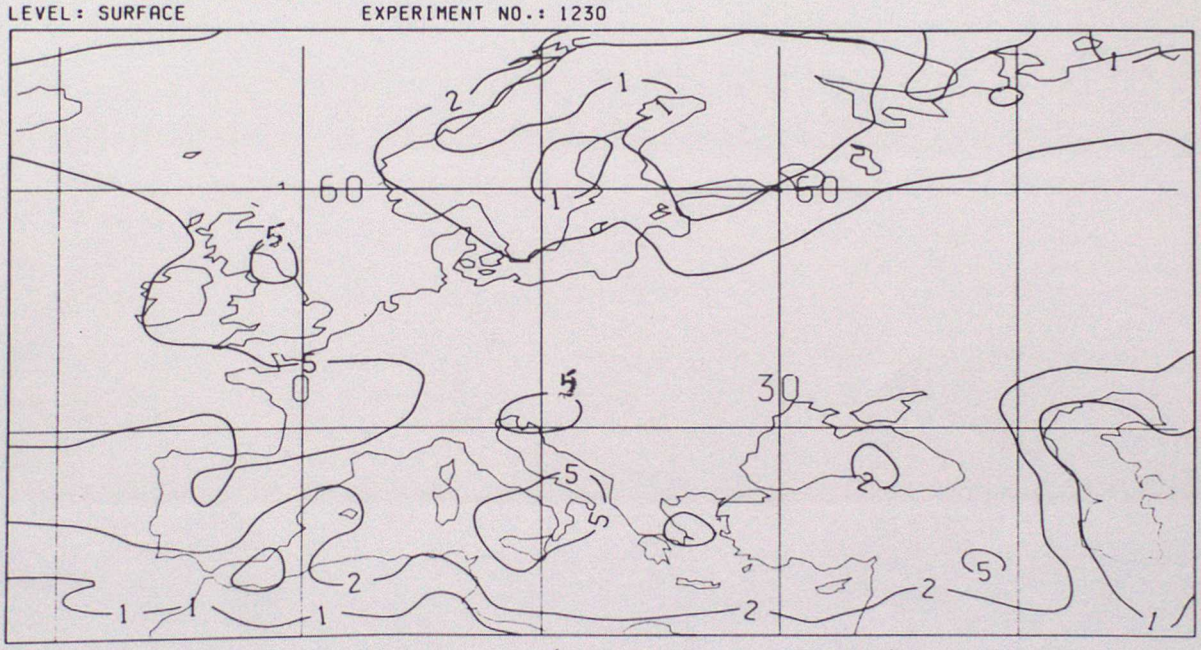

18c

PRECIPITATION DIFFERENCE (WAZF2150 - WAZG2150)

LEVEL: SURFACE

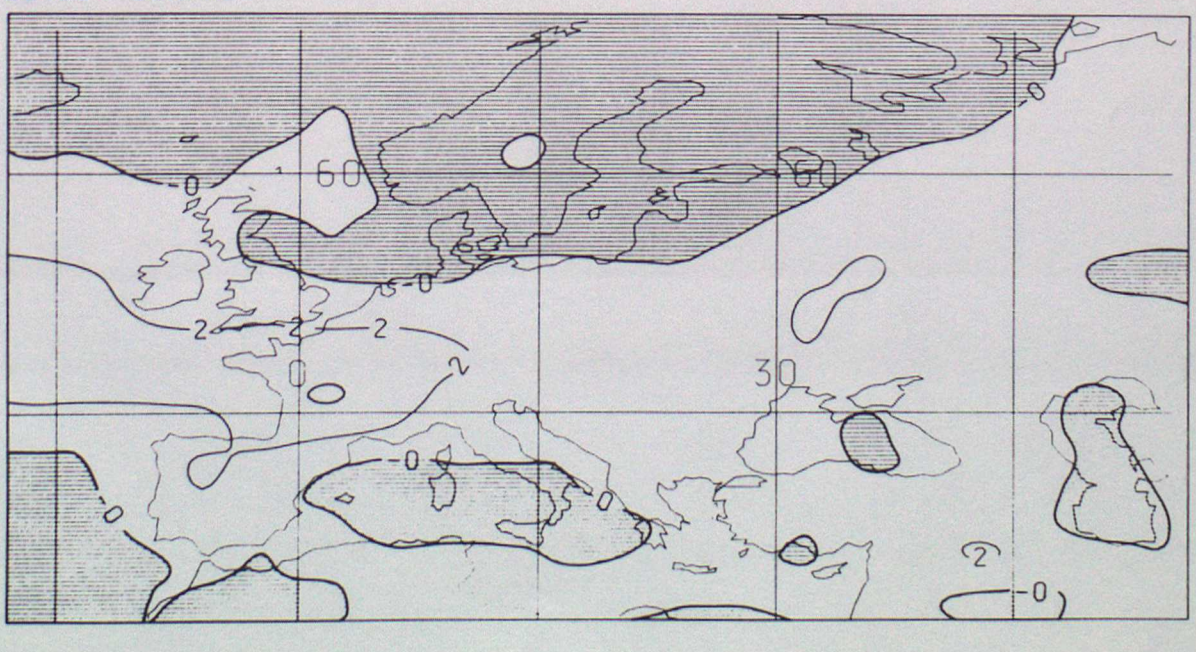

Figure 18: Precipitation in European area, a) WAZG2150, b) WAZF2150, c) WAZF2150 - WAZG2150.

18d

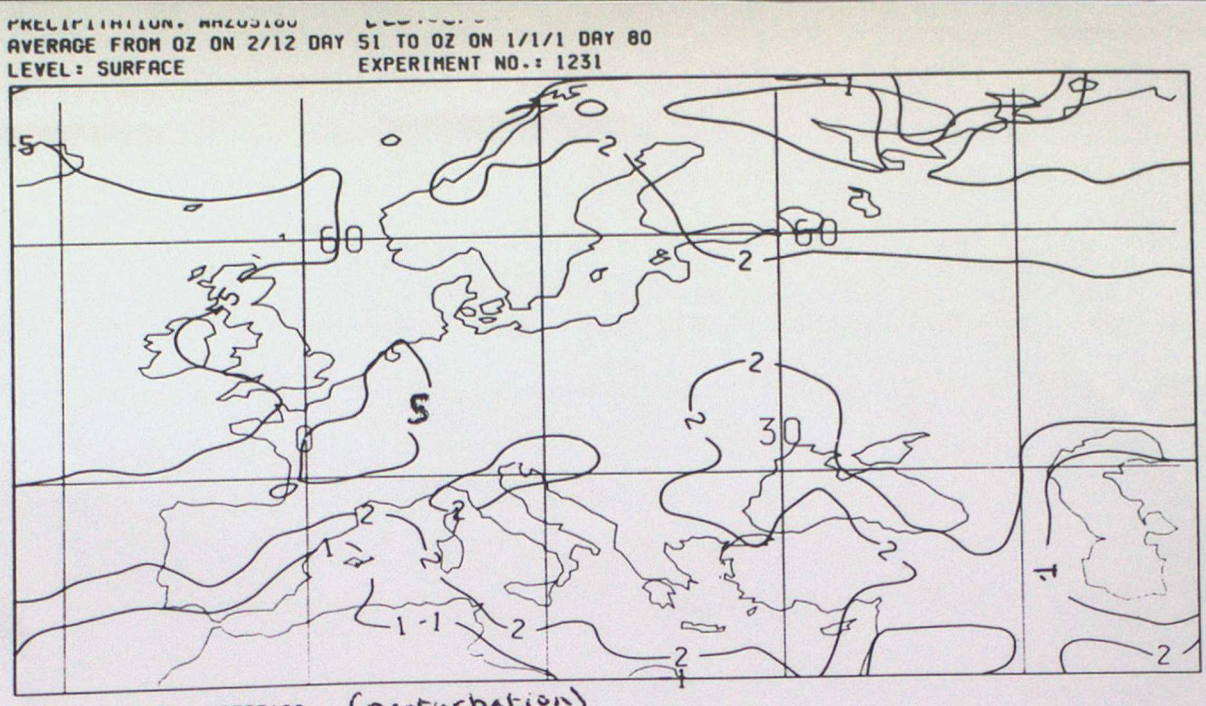

18e

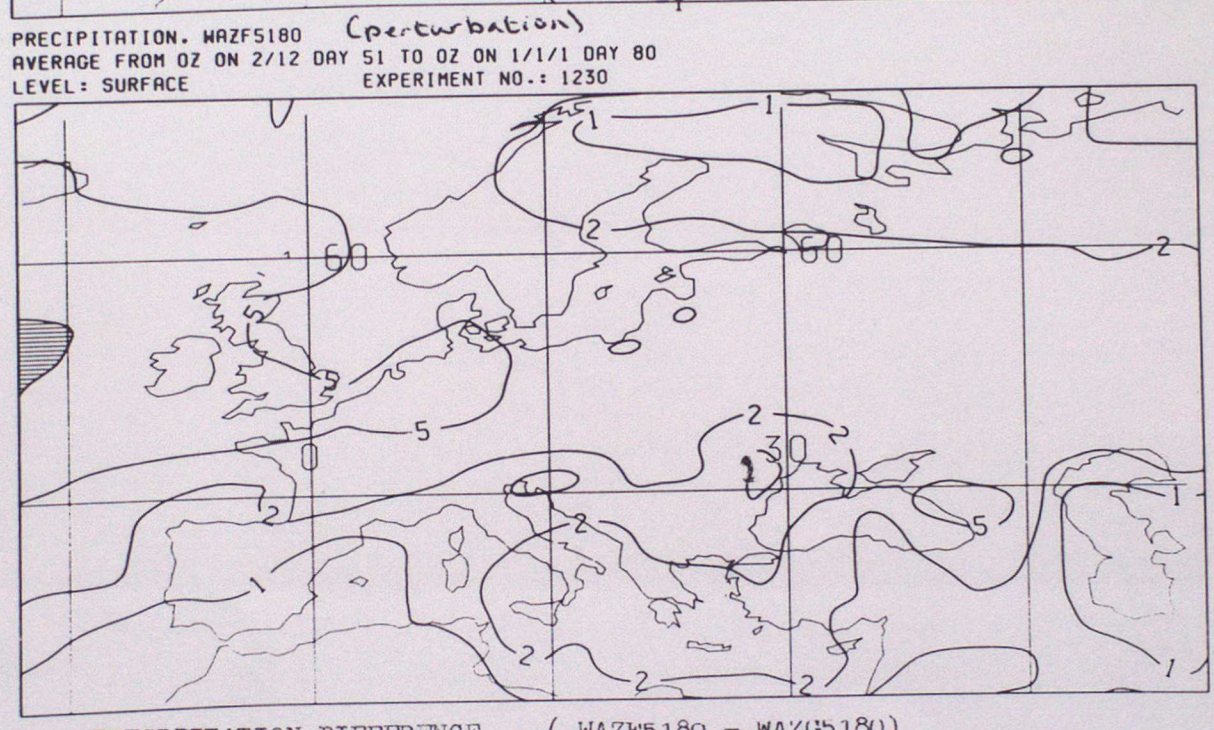

18f

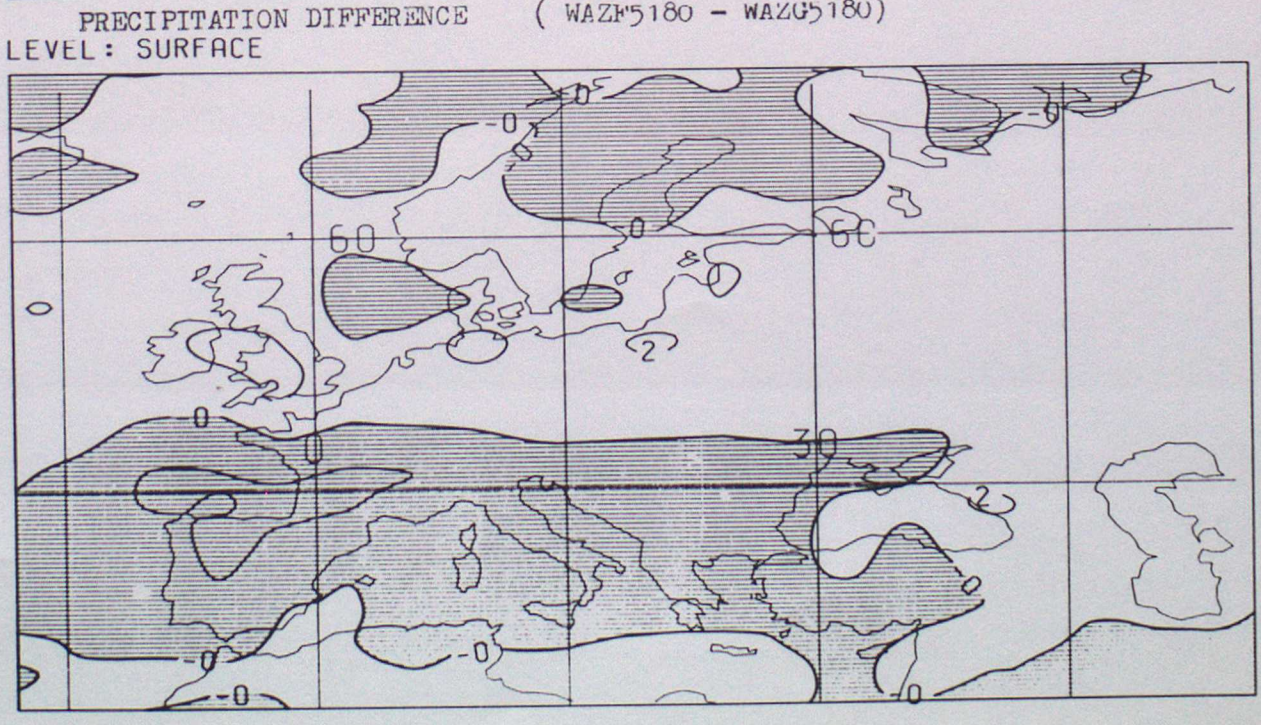

Figure 18: Precipitation in European area, d) WAZG5180, e) WAZF5180, f) WAZF5180 - WAZG5180.

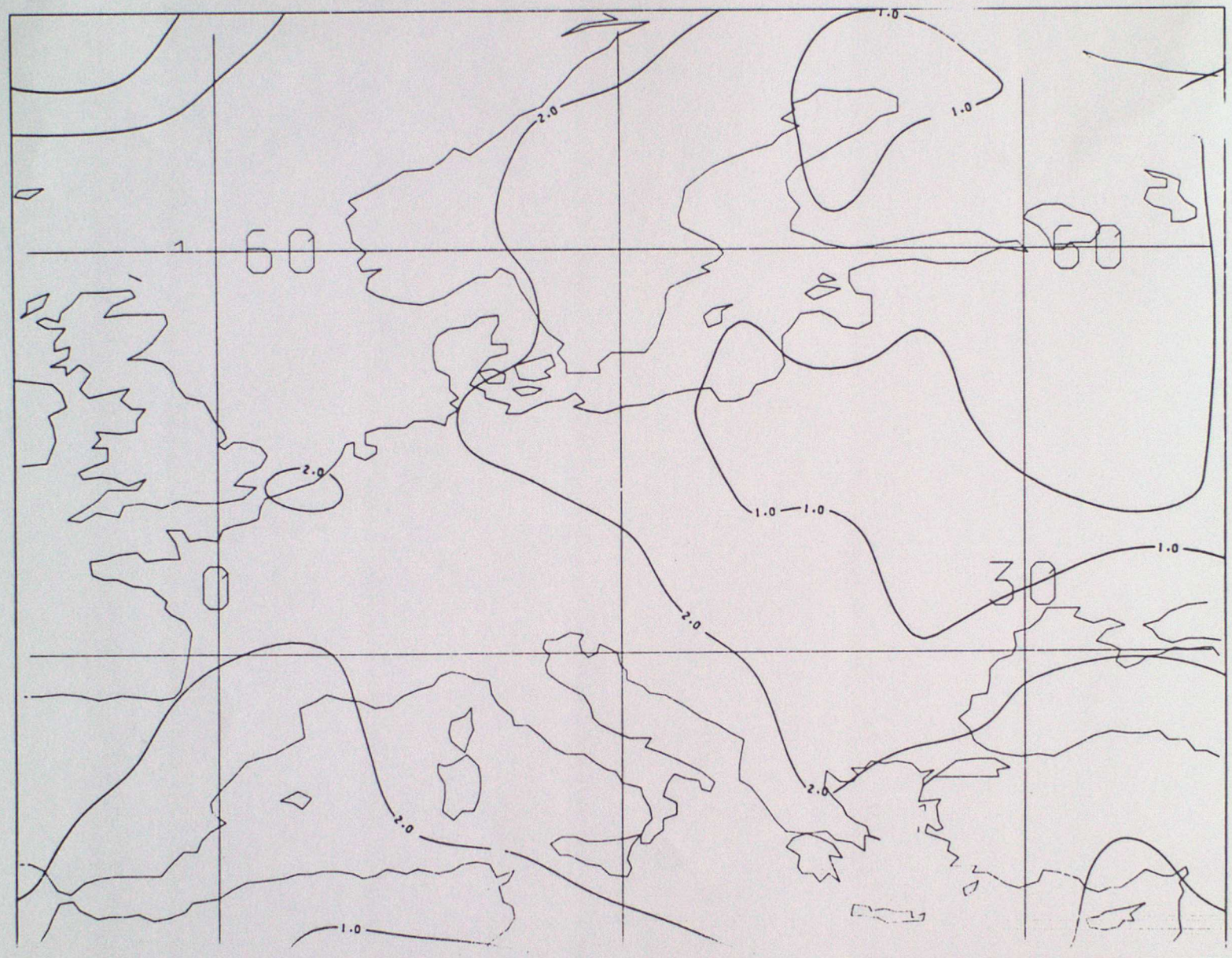

Figure 18: Climatological precipitation for January (mm/day), Jaeger (1983).

DYNAMICAL CLIMATOLOGY TECHNICAL NOTES

DCTN 1	June 1984	A scheme for incorporating the thermodynamic sea-ice model into a coupled ocean-atmosphere model. C Gordon and M Bottomley
DCTN 2	Sept 1984	The parametrization of the upper ocean mixed layer in coupled ocean/atmosphere models. C Gordon and M Bottomley
DCTN 3	Sept 1984	The response of a simple thermodynamic sea-ice model to GCM forcing appropriate for perennial sea-ice. M Bottomley
DCTN 4	Sept 1984	Potential vorticity in the stratosphere derived using data from satellites. S A Clough, N S Grahame and A O'Neill
DCTN 5	Sept 1984	Simulation of the seasonal cycle of SST using globally specified climatological data to force simple ocean models. N S Grahame
DCTN 6	Sept 1984	Development of an improved GCM radiation scheme. A Slingo and R C Wilderspin
DCTN 7	Sept 1984	On the specification of surface fluxes in coupled atmosphere/ocean general circulation models. J F B Mitchell, C A Wilson and C M Price
DCTN 8	Sept 1984	A survey of possible repercussions of the Soviet river reversal programme on Arctic sea-ice. H Cattle
DCTN 9	Oct 1984	A study of a strong stratospheric warming during January 1982 T D A Fairlie
DCTN 10	Nov 1984	An intercomparison of the Met O 11 N45 model and the Met O 20 11-level model on the Cyber 205 J F Dyson
DCTN 11	Nov 1984	Simulation of observed time series of temperature and precipitation over eastern England. D N Reed
DCTN 12	Nov 1984	Forecasts and analyses of the onset of the Southwest monsoon. R Kershaw
DCTN 13	Nov 1984	On modelling the effects of CO_2 on climate. J F B Mitchell
DCTN 14	Dec 1984	Development of a revised longwave radiation scheme for an atmospheric general circulation model. A Slingo and R C Wilderspin
DCTN 15	Jan 1985	Rossby wavetrains in the stratosphere forced by localised disturbances in the troposphere. C J Marks (Oxford), A O'Neill and V D Pope

DYNAMICAL CLIMATOLOGY TECHNICAL NOTES

DCTN 16	Jan 1985	Observing system experiments using the Meteorological Office's 15-level model. R A Bromley
DCTN 17	Feb 1985	Atmospheric general circulation simulation of the climate of the Mediterranean region. H Cattle
DCTN 18	Feb 1985	Diurnal variation and cloud in a general circulation model. C A Wilson and J F B Mitchell
DCTN 19	Feb 1985	The sensitivity of the Saharan region in a general circulation model. W M Cunnington and P R Rowntree
DCTN 20	Mar 1985	The impact of aircraft observations on analyses and forecasts from the operational 15-level model. B R Barwell
DCTN 21	Mar 1985	Non-linear effects on heat-induced circulation of the tropical atmosphere. A E Gill and P J Phlips
DCTN 22	Apr 1985	Simulation of cloudiness with the U.K. Meteorological Office 11-layer AGCM. A Slingo and R C Wilderspin
DCTN 23	Apr 1985	An integrated approach to the representation of cloud processes. R N B Smith
DCTN 24	May 1985	Nuclear Winter: Calculations of the shortwave radiative effects of soot aerosols. A Slingo and P Goldsmith
DCTN 25	Jul 1985	Sea ice and the Antarctic winter circulation: a numerical experiment. J F B Mitchell and T S Hills
DCTN 26	Jul 1985	A Budyko-Sellers model for study of ocean-atmosphere interaction. W J Ingram
DCTN 27	Aug 1985	The effect of a shoaling thermocline on equatorially-trapped Kelvin waves. A E Gill and B A King
DCTN 28	Sept 1985	CO_2 climate sensitivity and model dependence of results. J F B Mitchell, C A Wilson and W M Cunnington
DCTN 29	Sept 1985	Handbook of the Meteorological Office 11-layer atmospheric general circulation model. Volume 1 : Model Description Edited by A Slingo
DCTN 30	Sept 1985	Impact of land surface variations on African rainfall in general circualation models. P R Rowntree, M F Wilson and A B Sangster

DYNAMICAL CLIMATOLOGY TECHNICAL NOTES

DCTN 31	Nov	1985	The annual cycle of sea level in the eastern tropical Pacific. G R Bigg and A E Gill
DCTN 32	Nov	1985	An analytic model of the heat-induced tropical circulation in the presence of a mean wind. P J Phlips and A E Gill
DCTN 33	Nov	1985	The effect of resolution and diffusion on the simulated climate. J F Dyson
DCTN 34	Jan	1986	Rossby adjustment over a step. M K Davey, A E Gill, E R Johnson and P F Linden
DCTN 35	Jan	1986	Issues concerning the evaluation of effective surface roughness of heterogeneous terrain. D J Carson
DCTN 36	Mar	1986	Climate sensitivity and past climates : evidence from numerical studies J F B Mitchell
DCTN 37	Mar	1986	Parametrizations of land-surface processes in Meteorological Office numerical weather prediction and climate models D J Carson
DCTN 38	Apr	1986	Modelling of land-surface processes and their influence on European Climate D A Warrilow, A B Sangster and A Slingo
DCTN 39	Apr	1986	Simulation of climatic change due to increased CO_2 J F B Mitchell
DCTN 40	May	1986	On the interpretation of the Eliassen-Palm flux divergence. Part I : Theory D G Andrews
DCTN 41	June	1986	Experiments on tropical circulation with a simple moist model. M K Davey and A E Gill
DCTN 42	Jun	1986	Parameter regimes for studying isolated eddies. P D Killworth and M K Davey
DCTN 43	Jun	1986	A comparison of the impact of an envelope orography and of a parametrization of orographic gravity-wave drag on model simulations. A Slingo and D W Pearson
DCTN 44	Jul	1986	The effect of a sea-surface temperature anomaly on a prediction of the onset of the south-west monsoon over India. R Kershaw
DCTN 45	Jul	1986	An introduction to the parametrization of land-surface processes. D J Carson

DYNAMICAL CLIMATOLOGY TECHNICAL NOTES

DCTN 46	Sept	1986	Lateral boundaries and the heat-induced flow in the tropical atmosphere. P J Phlips and A E Gill
DCTN 47	Nov	1986	Simulation of the diurnal cycle of outgoing longwave radiation with an atmospheric GCM. A Slingo, R C Wilderspin and S J Brentnall
DCTN 48	Feb	1987	A 2 x CO_2 climate sensitivity experiment with a global climate model including a simple ocean C A Wilson and J F B Mitchell
DCTN 49	Feb	1987	Sensitivity of the Met O 20 11-layer model to increased land surface roughness length C C Heasman